THE ASTROPHYSICAL JOURNAL, 323:54-78, 1987 December 1

THE STRUCTURE OF YOUNG STAR CLUSTERS IN THE LARGE MAGELLANIC CLOUD

REBECCA A. W. ELSON,[1,2] S. MICHAEL FALL,[2,3] AND KENNETH C. FREEMAN[2,4]

Received 1987 February 9; accepted 1987 May 27

ABSTRACT

We present surface brightness profiles, based on star counts and aperture photometry, for 10 rich star clusters in the Large Magellanic Cloud, with ages between 8×10^6 and 3×10^8 years. The profiles extend over 8–10 mag in surface brightness, and to radii of 4′. Most of the clusters do not appear to be tidally truncated. At large radii the projected density falls off as $r^{-\gamma}$, with $2.2 \lesssim \gamma \lesssim 3.2$ and a median value $\gamma \approx 2.6$. With one possible exception, we find no evidence for mass segregation. To investigate the dynamical evolution of the clusters, we derive mass-to-light ratios from stellar population models. The estimated masses of the clusters are 10^4–10^6 $M_\odot$, where much of this range is due to uncertainties in the mass-to-light ratios. From the density profiles and the assumption of hydrostatic equilibrium, we calculate the velocity dispersion as a function of radius within the clusters. The predicted central velocity dispersions are 1–8 km s^{-1} in one dimension. The crossing times are shorter than the ages of the clusters, and the two-body relaxation times, except in a few of the cores, are considerably longer than the ages. Thus, the clusters are dynamically well mixed, but are not relaxed through stellar encounters. We consider various ways in which the clusters might have formed, and suggest several explanations for the observed profiles. Expansion of a newly formed cluster either through mass loss or during violent relaxation could lead to the formation of a halo of unbound stars. To examine this possibility, we include a calculation of the tidal field of the LMC. At least some and perhaps all the clusters in our sample extend beyond their eventual tidal radii, with up to 50% of the total masses in unbound halos.

Subject headings: clusters: globular — galaxies: Magellanic Clouds — stars: formation — stars: stellar dynamics.

I. INTRODUCTION

The evolution of globular clusters has been explored extensively over the past few decades (see Elson, Hut, and Inagaki 1987 and references therein). While increasingly detailed observations of the structure of globular clusters have shed light on their later evolution, two-body relaxation has obliterated most traces of their initial states. Thus, speculation concerning the early phases of cluster evolution, including the efficiency and rate at which a protocluster is converted into stars, the amount of dissipation during the initial collapse, the extent to which violent relaxation is successful in mixing the cluster, and the rate and way in which unbound stars are stripped from the cluster by the tidal field of the galaxy, remain largely untested.

The rich clusters in the Large Magellanic Cloud (LMC) provide an ideal opportunity to investigate these questions. Their ages span the full range from $\sim 10^6$ to $\sim 10^{10}$ yr; they are close enough to allow detailed studies of their stellar content but far enough away that their integrated properties may be determined relatively easily; obscuration by gas and dust is generally negligible; background/foreground crowding and membership determination are typically not severe problems; and they are on roughly circular orbits, so the effect of tidal forces on their structure may be quantified.

As a system, the LMC clusters bear more resemblance to open than to globular clusters in our Galaxy: their luminosity function and age distribution are at least qualitatively similar to those for our open clusters, and kinematically they are members of a disk population (Elson and Fall 1985*a*, *b*; Freeman, Illingworth, and Oemler 1983). However, some of the LMC clusters are considerably more massive than the open clusters in our Galaxy; the richest among them have $M \sim 10^5$ $M_\odot$, which is comparable to the masses of Galactic globular clusters.

Little work has been done on the structure of young star clusters in the LMC. Multiaperture photometry has been published for about a dozen of the clusters with ages $\lesssim 3 \times 10^8$ yr (Bernard and Bigay 1974; Gordon and Kron 1983). Freeman (1974), Chun (1978), and Nelson and Hodge (1983) have derived surface brightness profiles from drift scans and star counts for a total of four young clusters. As in most studies of Galactic globular clusters, tidally truncated King models were fitted to the observed profiles.

In this paper we present surface brightness profiles based on aperture photometry and star counts for 10 young clusters in the LMC. Our sample includes NGC 1818, NGC 1831, NGC 1866, NGC 2004, NGC 2156, NGC 2157, NGC 2159, NGC 2164, NGC 2172, and NGC 2214; these are typical of the richer clusters in the LMC. The profiles extend to surface brightnesses several magnitudes fainter than those of previous studies and provide interesting new constraints on ideas about the formation and early evolution of star clusters. The data are described and the profiles are presented in § II. To interpret the results in terms of the dynamical evolution of the clusters, we estimate their mass-to-light ratios from stellar population models in § III, and in § IV we calculate the tidal field of the LMC. In § V we derive spatial density profiles, total masses, and evolutionary time scales for the clusters. In § VI we interpret our results in terms of the formation and early evolution of rich star clusters.

Throughout this paper we adopt a distance modulus for the

[1] Institute of Astronomy, University of Cambridge, and Institute for Advanced Study, Princeton, New Jersey.
[2] Space Telescope Science Institute.
[3] Department of Physics and Astronomy, Johns Hopkins University.
[4] Mount Stromlo and Siding Spring Observatory, Australian National University.

LMC of 18.7, which corresponds to a distance of 55 kpc. There is some recent evidence, however, that the LMC may actually be closer by up to 10 kpc (Schommer, Olszewski, and Aaronson 1984; Chiosi and Pigatto 1986; Conti, Garmany, and Massey 1986). Adopting a smaller distance modulus would not alter our main conclusions; the effect on our estimates of various cluster properties is discussed where appropriate.

II. DATA AND CLUSTER PROFILES

To obtain surface brightness profiles for the young LMC clusters, we used a combination of aperture photometry and star counts. Both types of observations are necessary, since in the inner regions the clusters are too crowded to allow star counts, while in the outer regions the surface brightness is too faint compared with the background to use aperture measurements. The overall normalization of the profiles is determined from the photometry. For most of the clusters in our sample, the overlap regions, with both star counts and aperture photometry, are extensive enough to allow a reliable match in constructing composite profiles. An important assumption underlying such a hybrid approach is that the stars contributing most to the light and those contributing most to the counts have the same spatial distribution. In Galactic globular clusters, where similar methods are often used to obtain profiles, the giants, which contribute most of the light, have masses close to those of the brightest main-sequence stars, and thus probably have similar spatial distributions. For the young clusters studied here, the range of stellar masses is much greater (~ 1–$5\ M_\odot$); however, as discussed below, most of our star counts show no evidence for mass segregation. Frenk and Fall (1982) have measured the ellipticities of all the clusters in our sample. They find $\epsilon \lesssim 0.3$ in all cases and $\epsilon \lesssim 0.2$ in most cases, which is small enough to justify the approximation, made throughout, that the images of the clusters are round.

a) *Aperture Photometry*

For six of the clusters in our sample, NGC 2156, NGC 2157, NGC 2159, NGC 2164, NGC 2172, and NGC 2214, aperture photometry was obtained using the 0.6 m telescope at Siding Spring Observatory, with a 1P21 photomultiplier. Seven apertures ranging in diameter from 13.″3 to 112″ were used. Four independent measurements were made with each aperture, centered by eye on the clusters. Photometry was in the B and V bands; transformations to the Johnson system were made using E-region stars (Graham 1982), and zero points were fixed using the van Wijk sequence (Bok and Bok 1960). Backgrounds were determined for each cluster from four independent sky measurements, chosen far from the cluster, avoiding bright stars. The photometric errors are less than 2% (s.e.). For the remaining four clusters, integrated photometry was taken from the sources listed in Table 6 (p. 71); at least seven measurements, made with apertures ranging in diameter from 8″ to 204″, were available for each cluster. Values from different sources are in good agreement. Aperture magnitudes and $B - V$ colors for all the clusters are listed in Table 6; the magnitudes are plotted in the upper panels (*a*) of Figures 1–10.

The major sources of uncertainty in measurements made through large apertures are errors in the background determination and contamination by bright field stars; these are generally $\lesssim 0.1$ mag. One source of uncertainty in small-aperture measurements is centering. Hanes and Brodie (1985) find that the error introduced by miscentering apertures smaller than the cluster core is roughly independent of the aperture diameter, and that an offset of $0.4r_c$ would result in an underestimate of the magnitude by about 0.25 mag. In the photometry used here, the four independent measurements made with each aperture are in good agreement, suggesting that random centering errors are small. This does not, however, rule out the possibility that a small clump of bright stars was preferentially chosen as the cluster center. The major source of uncertainty in the small-aperture measurements is therefore stochastic fluctuations in the numbers of bright stars. Assuming that the fluctuations obey Poisson statistics, these errors may be estimated as in King *et al.* (1968). Representative errors, calculated from the data given by Robertson (1974*a*), are plotted in the upper panels (*a*) of Figures 1–10. In the fitting procedure described below, more weight was given to the photometry at intermediate radii.

b) *Star Counts*

The star counts were made from photographic plates in preference to CCD frames, because accurate determinations of the backgrounds are essential; a cluster and background field, which would require many CCD frames, are easily contained on a single photographic plate. The plates were obtained with either the 1 m telescope at Siding Spring Observatory or the 3.9 m Anglo-Australian Telescope. The limiting magnitudes were estimated by comparison with photoelectric sequences. They range from $B_{\rm lim} \approx 16$ to $B_{\rm lim} \approx 23$, which corresponds to the range of absolute magnitudes $-3 \lesssim M_B \lesssim +4$. For each cluster, between two and eight plates were counted, using a procedure similar to that described by King *et al.* (1968), Illingworth and Illingworth (1976), and DaCosta (1982). Circular reseaux, each with 30 annuli and 36 sectors, were centered by eye on the clusters, and stars were counted using a TV microscope and monitor, to facilitate counting to uniform limits. The plate scales s and reseaux diameters d for each plate are listed in Table 7 (p. 72).

The background density, f_b, on each plate, determined from the counts in the outer annuli, was subtracted from the total density to determine the cluster density, f_c. For the deepest plates, the cluster profiles are well defined out to $r_{\rm max} \approx 4'$, where f_c is less than 10% of f_b. The reseaux have radii of about 10′, so that there are ample counts in the outer annuli for the backgrounds to be determined accurately. The uncertainties in f_b are 1% in most cases and 5% in the worst cases. For the four clusters located close to one another (NGC 2156, NGC 2159, NGC 2164, and NGC 2172), care was taken in determining the backgrounds to exclude regions that might be contaminated by stars from neighboring clusters. For these clusters the four independent estimates of the backgrounds are equal to within 3% on the three deepest plates, indicating that contamination was successfully avoided. Finally, where necessary, crowding corrections were estimated using the empirical relation for "long-focus" plates given by King *et al.* (1968). The profiles are given in Table 7, where r is the radial range of the annuli in arcminutes, and f_c is the number of stars per square arcminute, after background subtraction but before crowding corrections.

c) *Composite Profiles*

Plots of the star counts indicated that the profiles were approximately power laws at large radii. We therefore fitted

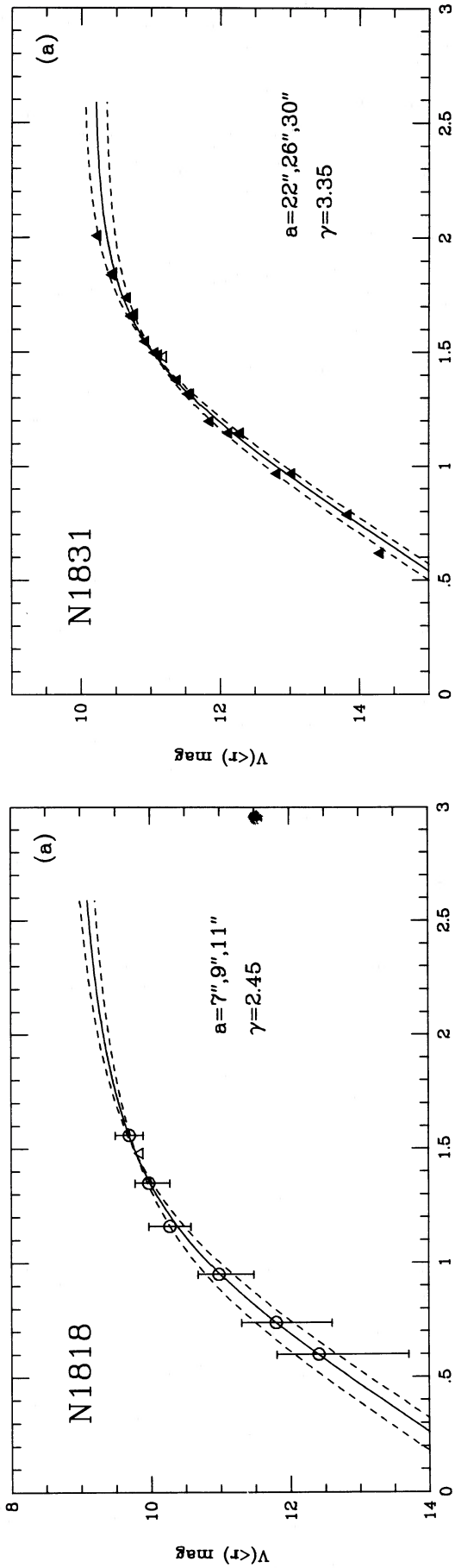

FIG. 1

FIG. 2

FIG. 1.—(*a*) Aperture photometry for NGC 1818. The data are listed in Table 6 and are from Gordon and Kron (1983) (*filled triangles*), van den Bergh and Hagen (1968) (*open triangles*), Bernard and Bigay (1974) (*open circles*), or this paper (*filled circles*). Representative error bars show the uncertainty due to stochastic fluctuations in the number of stars within an aperture. Solid and dashed curves are calculated from eq. (2) for the values of a and γ indicated. The solid curve represents the adopted parameters. (*b*) Star counts for NGC 1818. The plate corresponding to each symbol is indicated in Table 7; filled symbols are for deeper plates, while open symbols are for shallower plates. The scatter is comparable to the Poisson errors in the counts. Note the extensive radial overlap among the plates. The solid curve represents the model calculated from eq. (1) for the best-fit parameters. The upper arrow indicates the adopted value of a. The dashed curves are King models with core radius corresponding to a, and concentration c such that the cluster is tidally limited. The range in c reflects the uncertainties in M/L_V and in the tidal field of the LMC, as discussed in the text. The lower pair of arrows indicate the radius at which the velocity dispersion calculated from equation (16) drops to zero. The uncertainties are the same as for the King models.

FIG. 2.—Same as Fig. 1, but for NGC 1831

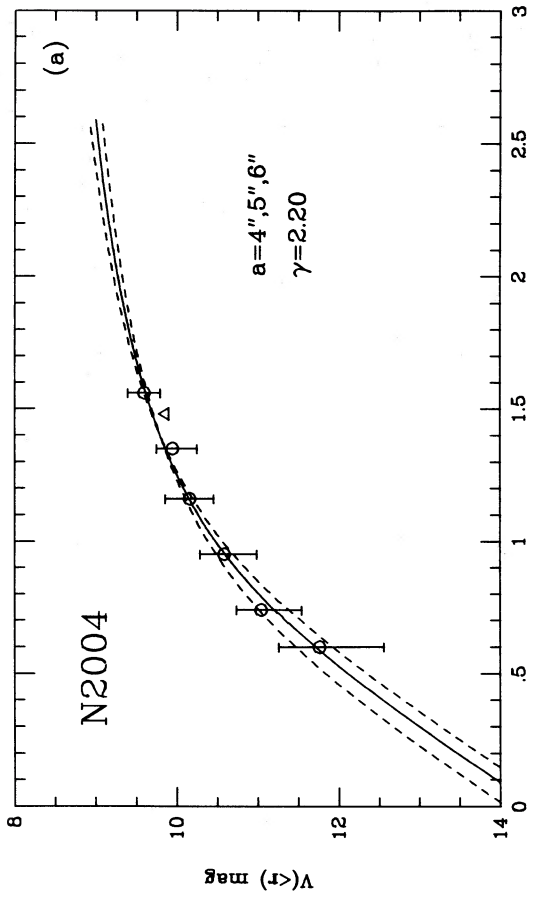

FIG. 3.—Same as Fig. 1, but for NGC 1866

FIG. 4.—Same as Fig. 1, but for NGC 2004

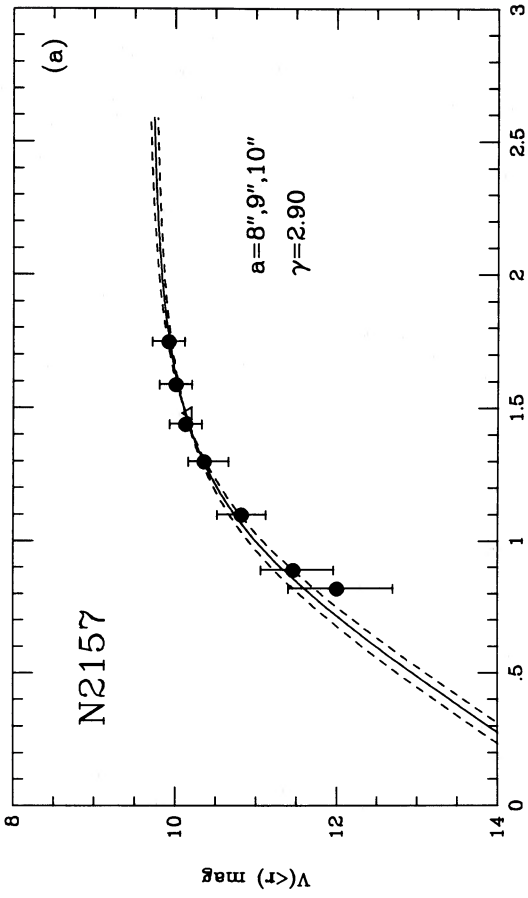

FIG. 6.—Same as Fig. 1, but for NGC 2157

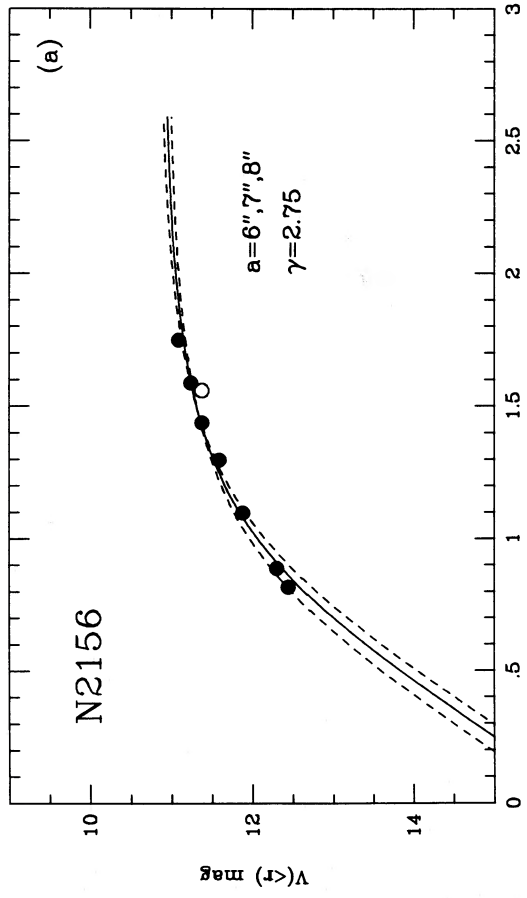

FIG. 5.—Same as Fig. 1, but for NGC 2156

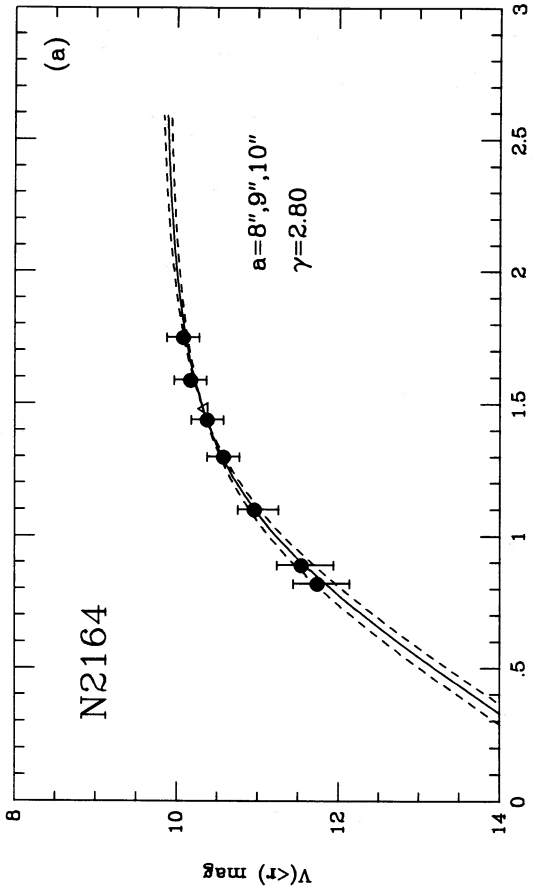

FIG. 8.—Same as Fig. 1, but for NGC 2164

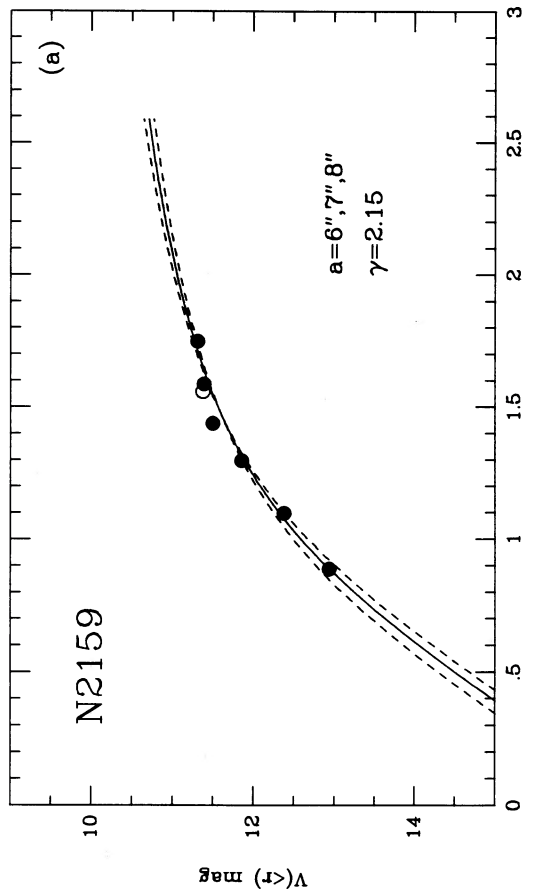

FIG. 7.—Same as Fig. 1, but for NGC 2159

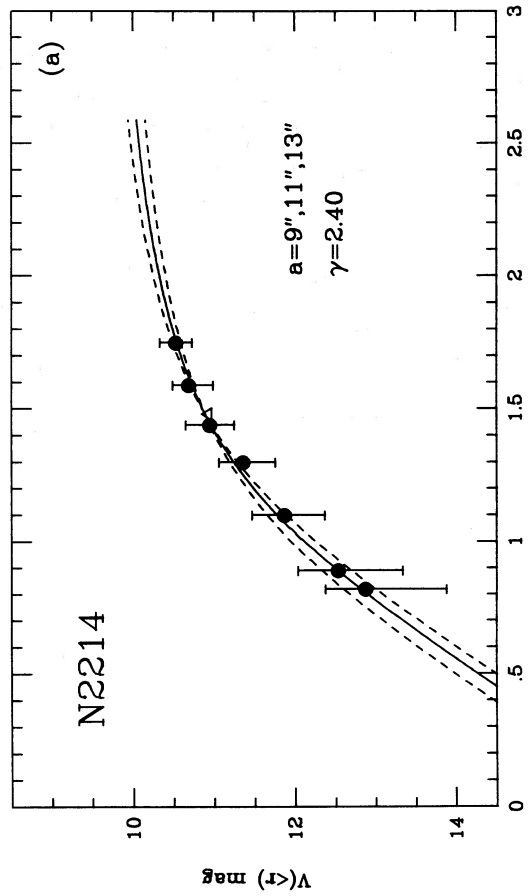

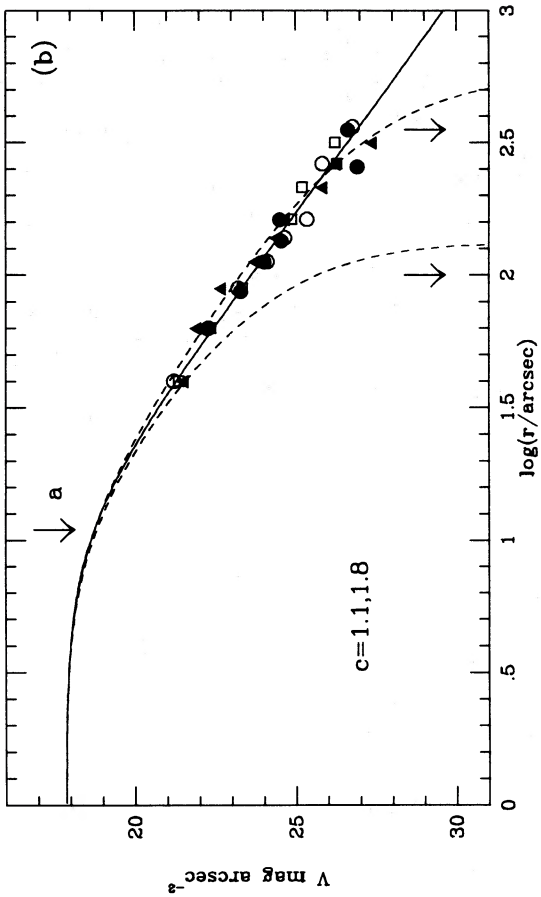

FIG. 10.—Same as Fig. 1, but for NGC 2214

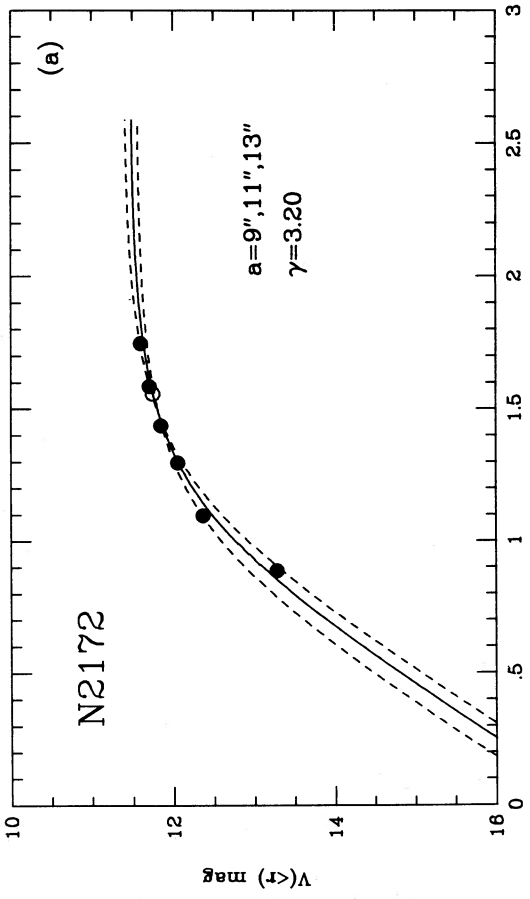

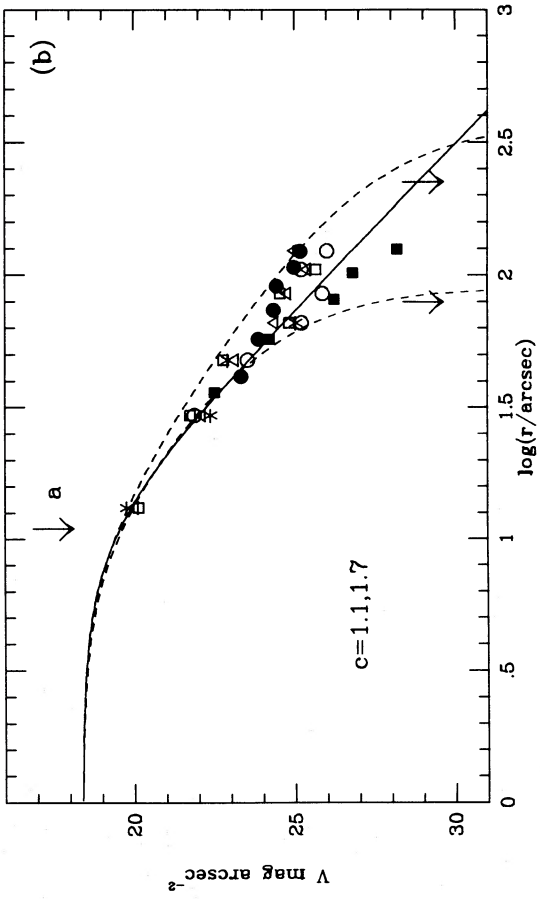

FIG. 9.—Same as Fig. 1, but for NGC 2172

the function

$$\mu(r) = \mu_0(1 + r^2/a^2)^{-\gamma/2} \quad (1)$$

to the observed profiles. This form was chosen purely for mathematical convenience; in § VI the profiles are discussed in the context of various physical models. Integrating equation (1) gives an expression for the luminosity within the projected radius r:

$$L_p(r) = \frac{2\pi\mu_0 a^2}{\gamma - 2}\left[1 - \left(1 + \frac{r^2}{a^2}\right)^{1-\gamma/2}\right]. \quad (2)$$

We first estimated a preliminary value of the index γ from all the star counts for each cluster. Equation (2) was then fitted by eye to the aperture photometry to estimate preliminary values of a and μ_0 (see the upper panels [a] of Fig 1–10). The relative shifts in $\log f_c$ from plate to plate, and an objective value of γ, were then determined by minimizing the statistic

$$\chi^2 = \sum_i \frac{(N_{\text{obs},i} - N_{\text{pred},i})^2}{N_{\text{obs},i}}, \quad (3)$$

where

$$N_{\text{obs},i} = A_i(f_{c,i} + f_b), \quad N_{\text{pred},i} = A_i(f_{p,i} + f_b).$$

In these expressions, $f_{p,i}$ is the density of cluster stars predicted by equation (1), and A_i is the solid angle subtended by the ith annulus. To find the best value of γ for each plate, equation (3) was summed only over the annuli on that plate. To find the best overall value of γ for each cluster, the sum was extended over all plates of that cluster. The procedure was then repeated, replacing the original value of γ with the one determined by minimizing χ^2, to obtain new values of μ_0 and a. Typically only one or two iterations were necessary before the solution converged.

Although the counts on deeper plates extend to somewhat larger radii, the common radial range for counts from all plates of a given cluster was generally at least half of the total range, allowing ample overlap for accurate alignment of the individual profiles. Comparison between the observed and expected χ^2 distributions for the combined set of all plates indicates that about 70% of the errors are accounted for by Poisson statistics alone. The uncertainties ϵ_j in the values of γ for each plate (shown in Fig. 11) are the 1 σ errors obtained from $\chi^2_{\min} + 1$ (see Avni 1976), added in quadrature with the uncertainty due to crowding. The latter is taken as the difference between the value of γ calculated with crowding corrections and that calculated without. In general, the contributions from the two sources are comparable. The error ϵ in the overall value of γ for each cluster was determined from the n plates by $\epsilon^{-2} = n^{-1}\sum \epsilon_j^{-2}$. The above procedure treats all the plates as independent. While this is not strictly correct, it avoids difficulties in combining plates with noncoincident radial bins.

The best-fit parameters of the composite profiles are listed in Table 1. The indices γ range from 2.2 to 3.2, with a median of 2.6 and a typical error of ± 0.3. The central surface brightnesses are in the range $1 \times 10^3 \lesssim \mu_0 \lesssim 2 \times 10^4\ L_\odot\ \text{pc}^{-2}$. They have been corrected for absorption adopting $E(B-V) = 0.10$, which is consistent with reddening values estimated from photometry of individual stars in or near each cluster (Heckman 1974; Robertson 1974*a*, *b*; Bok and Bok 1962; Persson *et al.* 1983). The values of a estimated from the aperture measurements vary in reliability; for NGC 1831 and NGC 1866, the ranges shown in Figures 2*a* and 3*a* are probably realistic. The intermediate values of a may be uncertain by up to 50%, and the smallest ones are very poorly determined. We emphasize that the aperture measurements are not suitable for detailed studies of the core regions of the clusters and are used primarily to fix the zero points of the surface brightness profiles. Typically the uncertainty in V_0 due to uncertainties in a is ± 0.2 mag.

TABLE 1

STRUCTURAL PARAMETERS

Cluster (NGC)	a	γ	$\log \mu_0$ ($L_\odot$ pc^{-2})	V_0 (mag arcsec^{-2})
1818	9″	2.45 ± 0.25	3.94	16.6
1831	26	3.35 ± 0.56	3.03	18.8
1866	17	2.55 ± 0.24	3.64	17.3
2004	5	2.20 ± 0.20	4.34	15.6
2156	7	2.75 ± 0.45	3.63	17.3
2157	9	2.90 ± 0.27	3.97	16.5
2159	7	2.15 ± 0.34	3.35	18.0
2164	9	2.80 ± 0.30	3.87	16.7
2172	11	3.20 ± 0.50	3.21	18.4
2214	11	2.40 ± 0.24	3.42	17.9

NOTE.—Structural parameters for the LMC clusters, obtained from eq. (1) as described in § II; μ_0 and V_0 have been corrected for absorption assuming $E(B-V) = 0.10$.

Figure 11 shows the value of γ determined for each plate plotted against the limiting magnitude of the plate. (Many of the B_{lim} values are preliminary.) There is no evidence for mass segregation in any of the clusters except perhaps NGC 1866. In this cluster the bright stars appear to be somewhat more centrally concentrated than the faint stars, and the adopted value of γ is appropriate for stellar masses in the range 1.5–4 $M_\odot$. We have also examined the $B-V$ colors in various annuli by differencing the aperture photometry. There are no obvious color gradients in any of the clusters, but the scatter is large, probably because of stochastic fluctuations in the numbers of bright stars, and could allow gradients as large as ± 0.003 mag arcsec^{-1}.

The composite profiles determined for the clusters using the procedure outlined above are shown in the lower panels (*b*) of Figures 1–10; they extend over 8–10 mag in surface brightness. The solid curves are the best-fit models, and the dashed curves are the King models discussed in § VI. Most of the profiles do not show the abrupt decrease that would be expected if the clusters were tidally limited. Previous profiles based on aperture photometry, drift scans, and star counts for NGC 1818, NGC 1866, and NGC 2157 (Freeman 1974; Chun 1978) agree well with our results, but the measurements do not extend to such large radii. In the case of NGC 2157, Chun found that the match between his star counts and drft scans was poor, and that the profile in the outer part of the cluster fell off less steeply than the best-fitting King model.

III. SYNTHETIC MASS-TO-LIGHT RATIOS

To study the dynamical evolution of the clusters, we need to know their mass profiles. If, as discussed above, mass segregation is negligible, then we can convert the luminosity profiles obtained in the previous section to mass profiles by simply multiplying by the appropriate mass-to-light ratio. Ideally, we would estimate mass-to-light ratios from the velocity dispersions in the clusters; such measurements are currently in

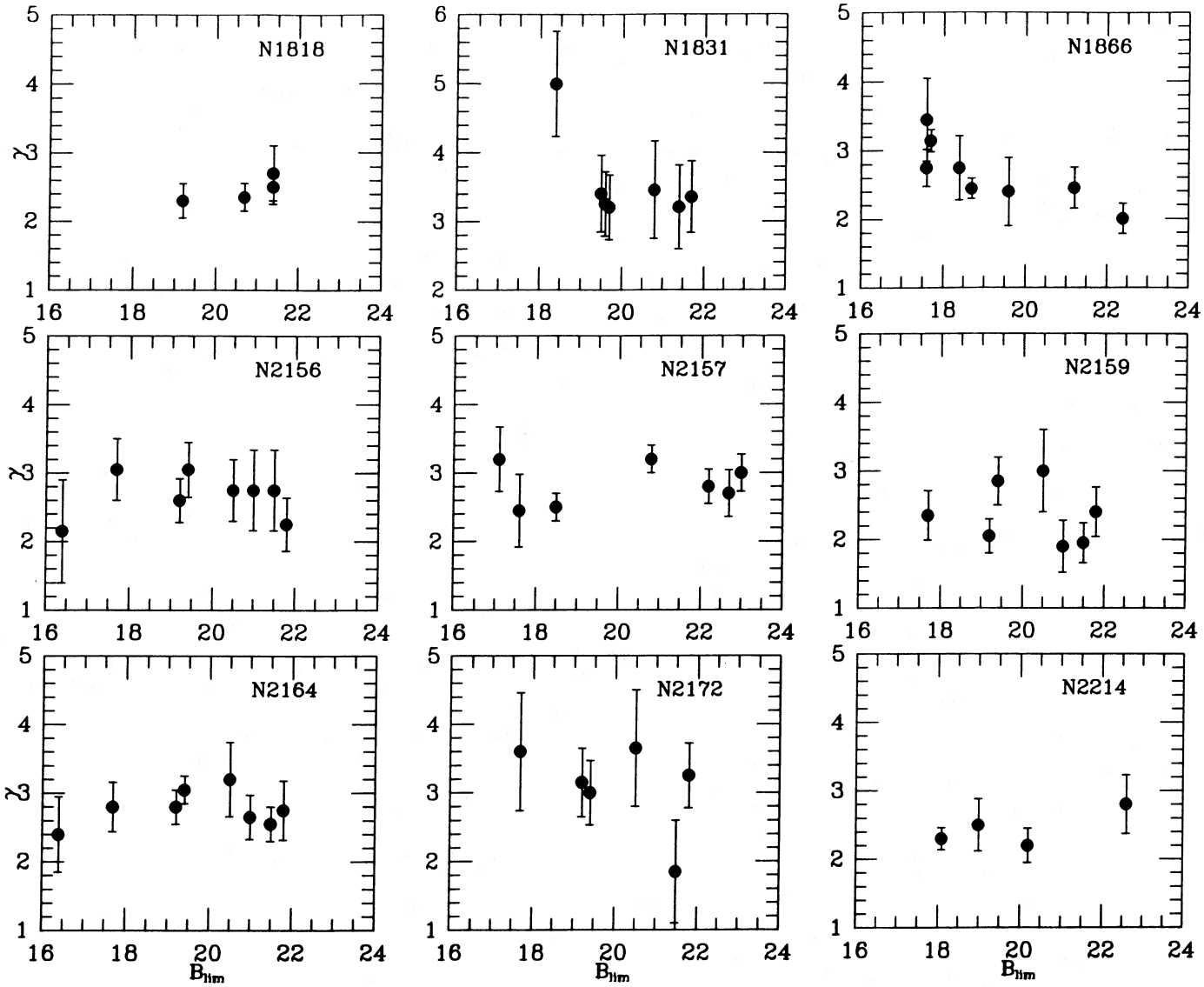

FIG. 11.—Power-law index γ plotted against limiting magnitude for each of the clusters. Error bars are calculated as described in § IIc.

progress for several LMC clusters, and the results will be reported in a separate paper. In the absence of dynamical mass-to-light ratios, we turn to stellar population models. The reverse procedure, using tidal radii to infer masses and hence mass-to-light ratios, is valid only for clusters sufficiently old that they are tidally truncated, and therefore cannot be applied to the clusters in our sample.

The total luminosity $L(\tau)$ of a single-burst stellar population in the V band is taken from the models of Searle, Sargent, and Bagnuolo (1973). These are based on isochrones from Iben (1965, 1966*a*, *b*, *c*, 1967) and Stothers (1963), include post–main-sequence evolution, and assume an initial mass function (IMF) of the form

$$\Phi(m) = \begin{cases} Am^{-(1+x)}, & m_l < m < m_u, \\ 0, & \text{otherwise}, \end{cases} \quad (4)$$

where $\Phi(m)dm$ is the number of stars formed in the mass interval $(m, m + dm)$. Searle *et al.* adopt $m_l = 0.25\ M_\odot$ and $m_u = 35\ M_\odot$ for the lower and upper cutoffs, and present results for three different IMF slopes: $x = 1.1$, $x = 1.45$, and $x = 2.2$. The IMFs for the clusters in our sample can be estimated from the star counts, and will be discussed in a later paper. However, at present only preliminary values of the magnitude limits of many of the plates are available. In converting the luminosities of the clusters to masses, we therefore allow the full range of IMF slopes considered by Searle *et al.*; this is consistent with the preliminary values reported by Freeman (1977) for six of the clusters in our sample.

To calculate the mass of the stellar population as a function of time, we have included the effect of mass loss due to stellar evolution, but not that due to the escape of stars from the cluster; in the absence of mass segregation, the escape of stars from a cluster would not affect its mass-to-light ratio. The total mass M is the sum of the mass in main-sequence stars, in remnants, and in evolved stars, although the latter is negligible; thus

$$M(\tau) = A \int_{m_l}^{m_t(\tau)} dm\ m^{-x} + A \int_{m_t(\tau)}^{m_u} dm\ m_{\rm rem}(m) m^{-(1+x)}\ . \quad (5)$$

For the dependence of the turnoff mass on age τ, we adopt (Renzini and Buzzoni 1986)

$$\log [m_t(\tau)/M_\odot] = 0.0558[\log (\tau/\mathrm{yr})]^2 - 1.338 \log (\tau/\mathrm{yr}) + 7.764 . \quad (6)$$

This is based on the isochrones of Becker and Iben (1979) and Mengel *et al.* (1979), and is in excellent agreement with the isochrones used by Searle *et al.* The mass of a white dwarf produced by a star with an initial mass m, for standard mass-loss rates, is given by (Iben and Renzini 1983)

$$m_{\mathrm{rem}}(m) = 0.38\ M_\odot + 0.15m . \quad (7)$$

The total masses of young clusters are not sensitive to the exact value of m_{rem}.

To determine the normalization constant A in equations (4) and (5), we equate

$$L(\tau) = A \int_{m_l}^{m_t(\tau)} dm\ l(m) m^{-(1+x)} \quad (8)$$

with the total luminosity given by Searle *et al.* Here $l(m)$ is the stellar mass-luminosity relation from the same models as used by Searle *et al.* The comparison was made at $\tau = 10^6$ yr, when even the most massive stars are still on the main sequence and the light from evolved stars is negligible. Figure 12 shows the resulting mass-to-light ratios as a function of time. Recent stellar population models of Yamanaka (1986), based on the Yale isochrones and calculated for the same parameters as above, are in excellent agreement with our results.

While the mass-to-light ratio is not sensitive to the upper cutoff of the IMF (for $1.1 \lesssim x \lesssim 2.2$), it depends strongly on the lower cutoff. Unfortunately, observations of LMC clusters are of little help in estimating the lower cutoff, since it is difficult to observe stars below about 1 $M_\odot$. In most Galactic globular clusters, the mass functions show no drastic lower cutoffs in the range 0.5–0.8 $M_\odot$ accessible to present observations (McClure *et al.* 1986). The mass function for field stars in the solar neighborhood appears to have a peak near 0.3 $M_\odot$ and probably falls off below 0.2 $M_\odot$ (Scalo 1986). Since the lower cutoff of the IMF may depend on environment, it could differ for cluster and field stars. The stippled region in Figure 12 indicates the uncertainty introduced by allowing the two extremes, $x = 1.1$ with $m_l = 0.5\ M_\odot$, and $x = 2.2$ with $m_l = 0.1\ M_\odot$. (In extrapolating the mass-to-light ratios of the models to these cases, we have neglected the small changes in the total luminosities.)

The ages of the clusters are taken from Hodge's (1983) compilation and are listed in Table 2. They are based on color-magnitude diagrams and the isochrones of Schlesinger (1969), Stothers (1972), and Brunish (1981). For the age range of our sample, 8×10^6 to 3×10^8 yr, these isochrones are in excellent agreement with the ones used in the stellar population models of Searle *et al.* The range in the mass-to-light ratio of each cluster, inferred from Figure 12, is listed in Table 3. Typically, half the uncertainty is due to the lower mass cutoff and half to the IMF slope. Adopting a distance modulus of 18.2 instead of 18.7 implies that the clusters are older by about 30%. The mass-to-light ratios predicted by the stellar population models therefore increase by about 20%, and since the absolute luminosities of the clusters decrease by 40%, the estimated masses decrease by 25%.

The models described above do not include convective overshooting, which may be important for stars with masses between 1.2 and 9 $M_\odot$. Thus, we have also plotted in Figure 12 a model calculated for a Salpeter IMF, with convective overshooting (Chiosi 1986; Chiosi, Bertelli, and Bressan 1986). This model predicts a lower M/L_V at a given age, but it also implies systematically larger ages (which are listed in Table 2), so that for a given cluster, the mass-to-light ratios predicted with and

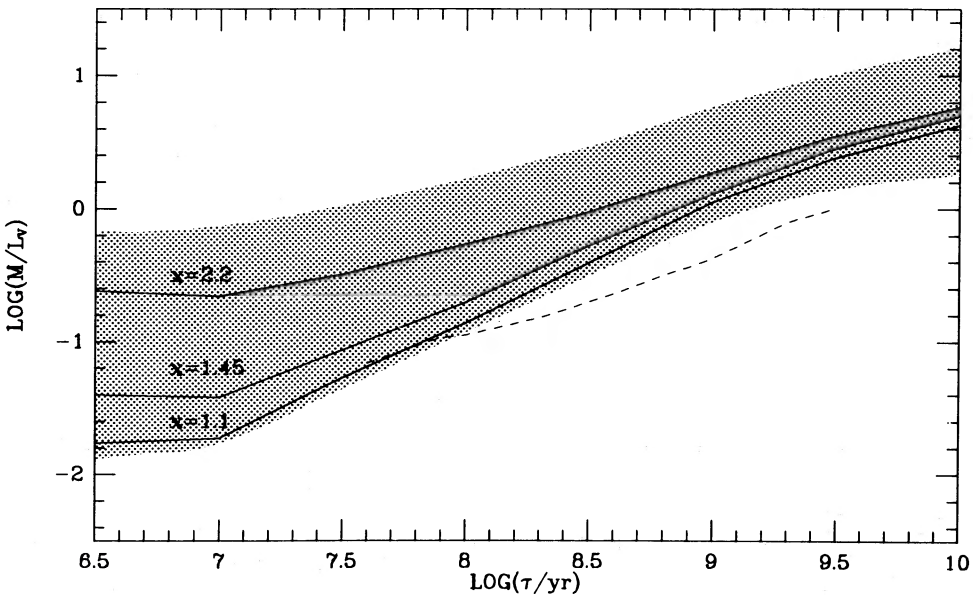

FIG. 12.—Mass-to-light ratio in solar units as a function of age for single-burst stellar populations. Solid curves are from the models of Searle, Sargent, and Bagnuolo (1973), with IMF slopes $x = 1.1$, $x = 1.45$, and $x = 2.2$, and lower and upper cutoffs $m_l = 0.25\ M_\odot$ and $m_u = 35\ M_\odot$. The stippled region indicates the uncertainty introduced by allowing the two extreme cases, $x = 1.1$ with $m_l = 0.5\ M_\odot$, and $x = 2.2$ with $m_l = 0.1\ M_\odot$. The dashed curve is from Chiosi's (1986) model with convective overshooting, and is calculated for $x = 1.35$ (see also Chiosi, Bertelli, and Bressan 1986). In all models, mass loss due to stellar evolution is calculated as described in § III. All models have a solar abundance of heavy elements.

TABLE 2

AGES AND TIME SCALES

Cluster (NGC) (1)	log τ (2)	log τ (3)	log τ_{orb} (4)	log $\tau_c(r_h)$ (5)	log $\tau_r(0)$ (6)	log τ_{rh} (7)
1818.....	7.2	8.0	8.4	6.2–7.0	8.2–8.8	9.0– 9.7
1831.....	8.3	8.8	8.6	6.5–7.0	9.1–9.5	9.6–10.0
1866.....	7.9	8.5	8.5	6.5–7.1	8.9–9.4	9.9–10.4
2004.....	6.9	7.7	8.3	6.3–7.2	7.7–8.4	9.1– 9.7
2156.....	7.8	8.3	8.5	6.1–6.7	8.0–8.5	8.7– 9.2
2157.....	7.5	8.5	8.5	6.1–6.8	8.2–8.7	8.9– 9.5
2159.....	7.8	8.3	8.5	6.4–7.1	8.0–8.4	9.0– 9.5
2164.....	7.7	8.3	8.5	6.1–6.7	8.2–8.7	9.0– 9.5
2172.....	7.8	8.3	8.5	6.3–6.9	8.2–8.6	8.8– 9.2
2214.....	7.6	8.3	8.7	6.6–7.3	8.2–8.8	9.4– 9.9

Col. (1).—Cluster name.

Col. (2).—Ages based on color-magnitude diagrams, from Hodge's 1983 compilation.

Col. (3).—Ages from Chiosi, Bertelli, and Bressan 1986, based on models that include convective overshooting.

Col. (4).—Orbital periods calculated using the galactocentric distances in Table 3 and the circular velocity from Fig. 13*a*.

Col. (5).—Crossing times at the median radii, calculated from eq. (18).

Col. (6).—Central relaxation times calculated from eq. (19).

Col. (7).—Reference relaxation times calculated from eq. (20).

NOTE.—The ranges in log $\tau_c(r_h)$, log $\tau_r(0)$ and log τ_{rh}, reflect uncertainties in the mass-to-light ratios. All times are in years.

without convective overshooting are approximately the same. All the models discussed above are for stellar populations with a solar abundance of heavy elements; this should be adequate, since the young LMC clusters have [Fe/H] ≈ -0.3 (Cohen 1982; Searle 1984). Models with this metallicity predict values of log (M/L_V) that differ by less than about 0.1 from the models with a solar abundance (Yamanaka 1986).

IV. TIDAL FIELD OF THE LARGE MAGELLANIC CLOUD

The surface brightness profiles shown in the lower panels (*b*) of Figures 1–10 suggest that most of the clusters in our sample are not yet tidally limited; however, if the clusters overflow their Roche lobes, then the unbound stars will eventually be stripped away. To quantify this effect, we now estimate the tidal field of the LMC and its uncertainties.

TABLE 3

GALACTOCENTRIC DISTANCES, TIDAL FIELD, AND MASS-TO-LIGHT RATIOS

Cluster (NGC) (1)	R (2)	$4\Omega^2 - \kappa^2$ (10^{-30} s^{-2}) (3)	log (M/L_v) (4)
1818	3°4	0.9–1.6	−1.7 to −0.1
1831	4.6	0.5–0.9	−0.7 to +0.3
1866	3.9	0.7–1.2	−1.1 to +0.1
2004	2.3	1.2–2.7	−1.9 to −0.2
2156	3.8	0.7–1.3	−1.1 to +0.1
2157	3.6	0.8–1.5	−1.4 to +0.0
2159	3.8	0.7–1.3	−1.1 to +0.1
2164	3.9	0.7–1.2	−1.2 to +0.1
2172	3.9	0.7–1.2	−1.1 to +0.1
2214	5.4	0.4–0.6	−1.3 to +0.0

Col. (1).—Cluster name.

Col. (2).—Galactocentric distances in the plane of the LMC, derived from the galactocentric distances in the plane of the sky given by Freeman, Illingworth, and Oemler 1983.

Col. (3).—Tidal field at the positions of the clusters from the stippled region in Fig. 13*c*.

Col. (4).—Mass-to-light ratios from the stippled region of Fig. 12.

The tidal acceleration of a star at a distance r from the center of a cluster is usually taken as the differential acceleration along a line joining the center of the cluster with the center of the galaxy. The result is $(4\Omega^2 - \kappa^2)r$, where Ω and κ are the circular and epicyclic frequencies of the galaxy at the pericenter of the orbit of the cluster (see King 1962). These are related to the circular velocity curve of the galaxy by

$$4\Omega^2 - \kappa^2 = -R \frac{d}{dR}\left[\frac{V(R)}{R}\right]^2 , \tag{9}$$

and $V(R)$ in turn is governed by the mass distribution. Thus, in determining the tidal field of the LMC, there are two possible starting points; its circular velocity curve may be deduced from the observed velocities of objects in the disk, or its mass distribution may be inferred from surface photometry, with some assumptions about the mass-to-light ratio.

In principle, the best approach is to use the rotation curve, because it reflects the total mass distribution including any dark matter than may be present. Rotation curves for the LMC based on observations of H I, star clusters, H II regions, planetary nebulae, and field stars have been published by Kerr and de Vaucouleurs (1955), Feast (1964), McGee and Milton (1966), Feitzinger (1979), and Rholfs, Kreitschmann, and Feitzinger (1984). In several cases there are substantial differences from one set of observations to the next. The data in Figure 13*a*, from Feitzinger (1979), are the mean results from a large sample of objects of all types, and are plotted assuming an inclination angle for the LMC of 30°. Unfortunately, all the available rotation curves are complicated by noncircular motions, probably induced by large expanding bubbles, the Bar, and, in the outer parts of the LMC, interactions with the SMC. The data for $R > 4°$ are based only on H I velocities. The rapid non-Keplerian falloff probably reflects motions of the Panmagellanic Gas, or the Magellanic Stream, and is not seen in other late-type spirals (Carignan and Freeman 1985). In estimating the tidal field, we therefore use only the position and amplitude of the peak of the rotation curve.

Surface photometry has the advantage that it is relatively easy to interpret, but the drawback that it only reflects the luminous component of the mass distribution. In Figure 13*b* we have plotted the *B*- and *R*-band measurements from de Vaucouleurs (1960). The photometry has been converted to a mass density assuming a mass-to-light ratio of 2.5 in *B* and 3.2 in *R*, consistent with the total mass implied by the peak of the rotation curves in Figure 13*a*. The absence of a color gradient is consistent with the assumption of a constant mass-to-light ratio across the disk.

The curves in Figures 13*a* and 13*b* are from two different models, both of which represent the observations adequately and are mathematically convenient. The solid curve is for an exponential disk with surface density

$$\mu(R) = \mu_E \exp(-\alpha R) , \tag{10a}$$

and the dashed curve is for a Kuz'min-Toomre disk with surface density

$$\mu(R) = \mu_K[1 + (\beta R)^2]^{-3/2} . \tag{10b}$$

The circular velocity curve for the exponential disk is given by

$$V^2(R) = \pi G \mu_E \alpha R^2 (I_0 K_0 - I_1 K_1)_{\alpha R/2} , \tag{11a}$$

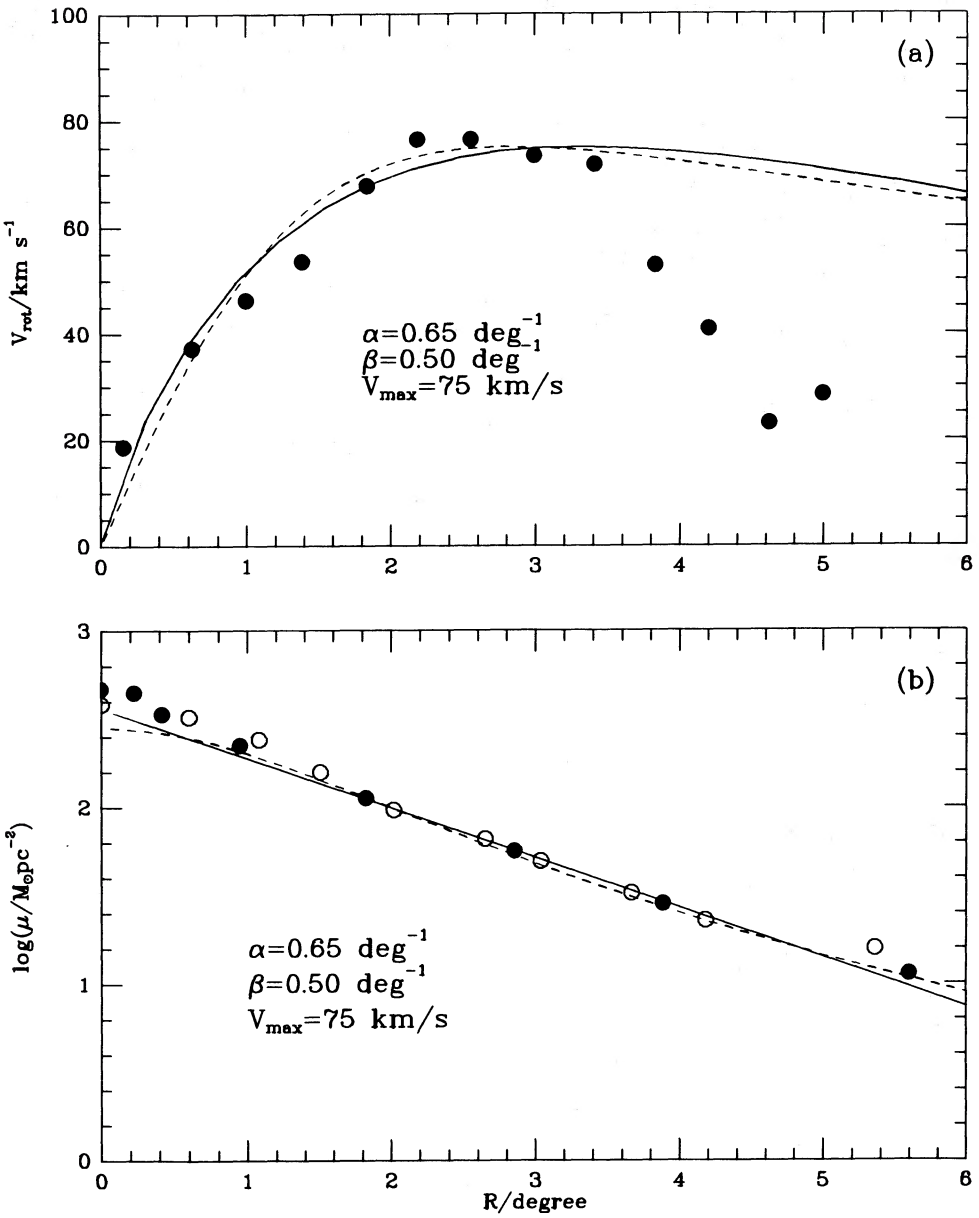

FIG. 13.—(*a*) Rotation curve for the LMC. Solid circles are from Feitzinger (1979); the abrupt decrease at $R > 4°$ is discussed in the text. The solid curve is for an exponential disk with $V_{max} = 75$ km s^{-1} and $\alpha = 0.65$ deg^{-1}, and the dashed curve is for a Kuz'min-Toomre disk with $V_{max} = 75$ km s^{-1}, and $\beta = 0.50$ deg^{-1}. (*b*) Surface density of the LMC. Solid circles are *B*-band photometry, and open circles, *R*-band photometry, from de Vaucouleurs (1960). The profiles have been converted to mass densities assuming $M/L_B = 2.5$ and $M/L_R = 3.2$. Solid and dashed curves are from the same models as in (*a*). (*c*) Tidal field of the LMC derived for the two models as described in § IV. Solid and dashed curves are from the same models as in (*a*) and (*b*). The stippled region includes the uncertainties in V_{max}, α, and β.

where I_n and K_n are modified Bessel functions of the first and second kind, of order n (Freeman 1970), and that for the Kuz'min-Toomre disk is given by

$$V^2(R) = 2\pi G\mu_K \beta R^2[1 + (\beta R)^2]^{-3/2} \qquad (11b)$$

(Toomre 1963). The circular velocity curves have maxima of $V_m = 1.56(G\mu_E/\alpha)^{1/2}$ at $R_m = 2.15/\alpha$, and $V_m = 1.56(G\mu_K/\beta)^{1/2}$ at $R_m = 1.41/\beta$, for the exponential and Kuz'min-Toomre disks, respectively.

The tidal fields for the two models, from equation (9), are

$$4\Omega^2 - \kappa^2 = \pi G\mu_E \alpha^2 R(I_0 K_1 - I_1 K_0 - 2I_1 K_1/\alpha R)_{\alpha R/2} \qquad (12a)$$

and

$$4\Omega^2 - \kappa^2 = 6\pi G\mu_K \beta^3 R^2[1 + (\beta R)^2]^{-5/2} . \qquad (12b)$$

Feitzinger's rotation curve, and those of the other authors

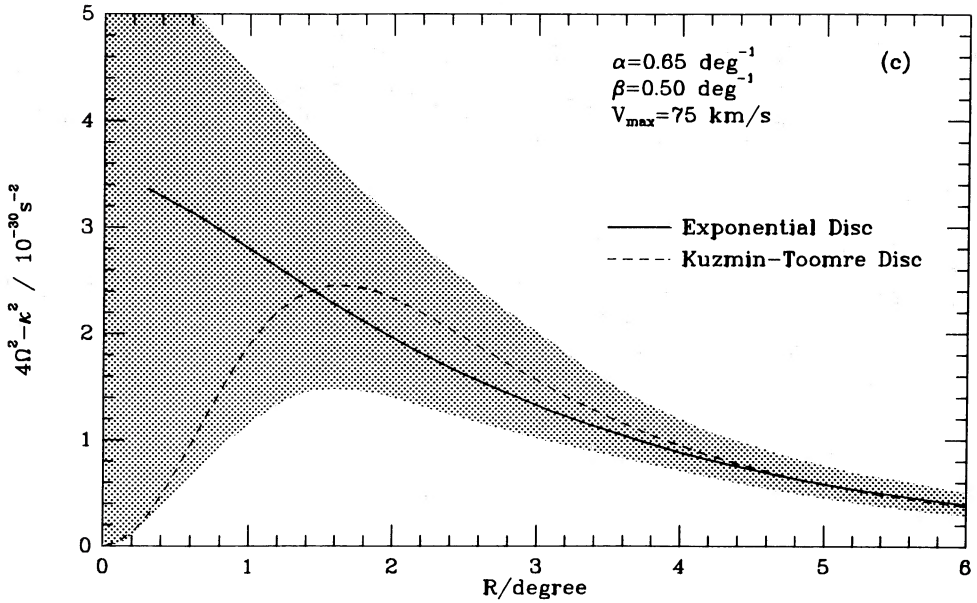

FIG. 13.—*Continued*

mentioned above, are all consistent with $V_{max} = 75 \pm 10$ km s^{-1}, assuming an inclination angle of 30° ± 3°, and these are the values we adopt. The surface photometry alone implies best values of $\alpha = 0.72$ deg^{-1} and $\beta = 0.55$ deg^{-1}; the rotation curve alone implies $\alpha = 0.60$ deg^{-1} and $\beta = 0.45$ deg^{-1}. Fitting the models to both the surface photometry and the rotation curve yields the following best values: $\alpha = 0.65 \pm 0.05$ deg^{-1} and $\beta = 0.50 \pm 0.05$ deg^{-1}. The implied total mass of the LMC is in the range (3–9) × 10^9 $M_\odot$.

The resulting tidal fields are plotted in Figure 13*c*. Although the available surface photometry and rotation curve cannot distinguish between the models, they imply vastly different behavior in the tidal field at $R \lesssim 2°$. The reason for this is that the Kuz'min-Toomre disk has solid-body rotation at small R, whereas the exponential disk has $V^2(R) \approx \pi G \mu_E \alpha R^2 \ln(2/\alpha R)$ for $\alpha R \ll 1$. The photometry near the center of the LMC resembles more closely the exponential disk, so the uncertainties may have been overestimated at small R. For $\alpha R \gtrsim 1$ or $\beta R \gtrsim 1$, the tidal fields of the two models are very similar, and the main source of uncertainty, indicated by the stippled region, is the uncertainty in V_{max}, α, and β, due principally to uncertainties in the inclination angle of the LMC. All the clusters in our sample are at $R > 2°$, where the uncertainty in the tidal field is less than 50%. The distances of the clusters from the center of the LMC, and the adopted values of the tidal field at their positions, are listed in Table 3.

V. MASS DISTRIBUTIONS AND EVOLUTIONARY TIME SCALES

a) Mass Distributions

The mass per unit volume in a cluster, $\rho(r)$, may be calculated by deprojecting equation (1) and multiplying by the appropriate mass-to-light ratio. The deprojected profiles have the same functional form as the projected profiles, but with index $\gamma + 1$:

$$\rho(r) = -\frac{1}{\pi}\frac{M}{L}\int_r^\infty dx (x^2 - r^2)^{-1/2}\frac{d\mu(x)}{dx} = \rho_0\left(1 + \frac{r^2}{a^2}\right)^{-(\gamma+1)/2}, \quad (13a)$$

where

$$\rho_0 = \frac{\mu_0 \Gamma(\gamma/2 + 1/2)}{\sqrt{\pi}\, a \Gamma(\gamma/2)}\frac{M}{L}, \quad (13b)$$

and Γ denotes the usual gamma function. The central densities of the clusters, derived from the mass-to-light ratios in Table 3, are listed in Table 4. Typically the clusters in our sample have $\rho_0 \sim 10^2$–10^3 $M_\odot$ pc^{-3}. For comparison, the distribution of central densities for Galactic globular clusters peaks at $\rho_0 \sim 10^3$–10^4 $M_\odot$ pc^{-3} (Webbink 1985), the Hyades open cluster has $\rho_0 \sim 3$ $M_\odot$ pc^{-3} (Pels, Oort, and Pels-Kluyver 1975), the Pleiades has $\rho_0 \sim 10$ $M_\odot$ pc^{-3} (van Leeuwen 1980), and the rich open cluster M11 has $\rho_0 \sim 4 \times 10^2$ $M_\odot$ pc^{-3} (Mathieu 1984). With a distance modulus of 18.2, the inferred linear sizes in the LMC would decrease by 20%. Since, as discussed above, the masses would decrease by 25%, the spatial densities of LMC clusters would increase by about 50%.

The total mass within a radius r is obtained by integrating equation (13a); in the limit $r \to \infty$, and for $\gamma > 2$, we obtain

$$M_\infty = \frac{2\pi\mu_0 a^2}{\gamma - 2}\frac{M}{L}. \quad (14)$$

The "asymptotic" mass of each cluster is listed in Table 4: the values range from $\sim 10^4$ to $\sim 10^6$ $M_\odot$, which is well above the typical masses of the open clusters in the disk of our Galaxy,

TABLE 4

LUMINOSITIES, MASSES, AND CENTRAL PARAMETERS

Cluster (NGC) (1)	$\log L_{max}$ ($L_\odot$) (2)	$\log L_\infty$ ($L_\odot$) (3)	$\log M_\infty$ ($M_\odot$) (4)	$\log \rho_0$ ($M_\odot$ pc^{-3}) (5)	σ_0 (km s^{-1}) (6)
1818	5.70	5.84	4.1–5.7	1.6–3.2	1.1–6.8
1831	5.35	5.38	4.7–5.7	1.3–2.3	1.9–6.0
1866	5.92	6.01	4.9–6.1	1.6–2.8	2.1–8.3
2004	5.78	6.09	4.2–5.9	2.0–3.7	1.0–7.3
2156	5.05	5.09	4.0–5.2	2.0–3.2	1.3–5.2
2157	5.54	5.57	4.2–5.6	2.0–3.4	1.5–7.6
2159	5.10	5.51	4.4–5.6	1.7–2.9	1.0–4.0
2164	5.48	5.52	4.3–5.6	2.1–3.4	1.7–7.7
2172	4.83	4.86	3.8–5.0	1.5–2.7	1.0–3.9
2214	5.42	5.55	4.3–5.6	1.4–2.7	1.0–4.7

Col. (1).—Cluster name.

Col. (2).—Integrated luminosity within a sphere of radius r_{max}.

Col. (3).—Asymptotic luminosity.

Col. (4).—Asymptotic mass, calculated from L_∞ and the mass-to-light ratios in Table 3.

Col. (5).—Central mass density.

Col. (6).—Central one-dimensional velocity dispersion, calculated from eq. (16).

NOTE.—The ranges in $\log M_\infty$, $\log \rho_0$, and σ_0 reflect uncertainties in the mass-to-light ratios. Luminosities are corrected for absorption assuming $E(B-V) = 0.10$.

and is comparable to the masses of Galactic globular clusters. We note, however, that the clusters in our sample are among the richest in the LMC, which also contains a large population of faint clusters (see Elson and Fall 1985*b*). Values of L_{max}, the total luminosity within a sphere of radius r_{max} (the radial extent of the star counts) are also listed in Table 4. They are typically smaller than L_∞ by 10%, but for clusters with shallower profiles, the difference may be as much as 50%. The asymptotic luminosities are 0.5–1.5 mag brighter than the photoelectric measurements compiled by van den Bergh (1981), which were made with apertures 40″–80″ in diameter.

b) Evolutionary Time Scales

To understand the structure and evolution of the young LMC clusters, we must determine the regions in which orbital mixing and two-body relaxation have been important. These depend on the velocities of the stars within the clusters. For a spherical cluster in hydrostatic equilibrium, the velocity dispersion in the radial and tangential directions, σ_r and σ_t, are related to the density by

$$\frac{1}{\rho}\frac{d}{dr}(\rho\sigma_r^2) + \frac{2}{r}(\sigma_r^2 - \sigma_t^2) = -\frac{GM(r)}{r^2} + (4\Omega^2 - \kappa^2)r\,. \quad (15)$$

The first term on the right-hand side of this equation arises from the self-gravity of the cluster. The second term is from the tidal field of the parent galaxy, as discussed in § IV. It gives the correct tidal stretching along the line joining the center of the cluster with the center of the LMC, but ignores the compression in the orthogonal direction and therefore is only approximately correct for the cluster as a whole. Nevertheless, equation (15) does give the correct velocity dispersion in the inner parts of the cluster, where tidal effects are small.

The velocity distributions in the outer parts of the LMC clusters may be anisotropic; however, in the absence of observations that allow us to quantify the amount of anisotropy, we assume $\sigma_r = \sigma_t = \sigma$. Note that, while there is a large radial anisotropy observed in the outer parts of the Pleiades (Jones 1970), there is little anisotropy in Praesepe (Jones 1971). With the density profile given by equations (13a) and (13b), the solution of equation (15) is

$$\sigma^2(r) = \frac{G}{a}\left(1 + \frac{r^2}{a^2}\right)^{(1+\gamma)/2} I\left(\frac{r}{a}\right) - \frac{a^2(4\Omega^2 - \kappa^2)}{(\gamma - 1)}\left(1 + \frac{r^2}{a^2}\right), \quad (16)$$

where

$$I(x) = \int_x^\infty \frac{M(ay)dy}{y^2(1 + y^2)^{(\gamma+1)/2}}\,. \quad (17)$$

Figure 14*a* shows σ as a function of r for several different values of γ, calculated without the tidal term in equation (16). The velocity dispersions are roughly constant for $r \lesssim a$ and decrease slowly at larger radii. Figure 14*b* shows $\sigma(r)$ calculated with a representative, nonzero value of $(4\Omega^2 - \kappa^2)/G\rho_0$ in equation (16). The tidal field of the LMC has little effect at $r \lesssim 5a$, but outside this radius it causes an abrupt decrease in the velocity dispersion.

The predicted central velocity dispersions of the clusters in our sample are listed in Table 4. We find $\sigma_0 \approx 1$–8 km s^{-1}, where most of this range is due to the uncertainties in the mass-to-light ratios. For comparison, Galactic globular clusters have $\sigma_0 \sim 10$ km s^{-1} (Illingworth 1976), and Galactic open clusters have $\sigma_0 \sim 1$ km s^{-1} (Mathieu 1985 and references therein). The radius at which $\sigma = 0$ for each cluster is listed in Table 5 and indicated by the arrows in the lower panels (*b*) of Figures 1–10. This is where the assumption of hydrostatic equilibrium, and hence the validity of equation (15), breaks down. It may also be an indication of the eventual tidal radius because $\sigma(r)$ declines so rapidly in the outer parts of a cluster that the pressure gradient $d(\rho\sigma^2)/dr$ vanishes at nearly the same radius. (For a King [1966] model, $\sigma = 0$ occurs precisely at the tidal radius.)

To estimate the degree of orbital mixing in the clusters, we adopt the following definition of the crossing time:

$$\tau_c(r_h) = \frac{2r_h}{\sqrt{3}\,\sigma(r_h)}\,, \quad (18)$$

TABLE 5

LENGTH SCALES

Cluster (NGC) (1)	$\log r_c$ (2)	$\log r_h$ (3)	$\log r_{max}$ (4)	$\log r_{\sigma=0}$ (5)	$\log r_t$ (6)
1818	0.89	1.45–1.75	2.3	1.9–2.5	1.9–2.7
1831	1.27	1.65	2.4	2.2–2.7	2.3–2.8
1866	1.16	1.80	2.7	2.2–2.7	2.3–2.9
2004	0.67	1.50–2.30	2.3	1.7–2.5	1.8–2.7
2156	0.75	1.25	2.3	1.9–2.4	2.0–2.6
2157	0.85	1.35	2.4	2.0–2.5	2.1–2.8
2159	0.82	1.45–2.85	2.4	1.8–2.4	1.9–2.6
2164	0.86	1.35	2.4	2.0–2.6	2.2–2.8
2172	0.91	1.35	2.1	1.9–2.4	2.0–2.6
2214	0.99	1.65–2.35	2.6	2.0–2.6	2.1–2.8

Col. (1).—Cluster name.

Col. (2).—Core radius calculated from eq. (22).

Col. (3).—Median radius, calculated for L_{max} and L_∞ (where only one value is given, the two are equal to within the uncertainties).

Col. (4).—Radial extent of the star counts.

Col. (5).—Radius at which $\sigma = 0$, calculated from eq. (16).

Col. (6).—Tidal radius of the King models plotted in the lower panels (*b*) of Figs. 1–10.

NOTE.—The ranges in $\log r_{\sigma=0}$ and $\log r_t$ reflect uncertainties in the mass-to-light ratios and the tidal field of the LMC. All radii are in arcsec.

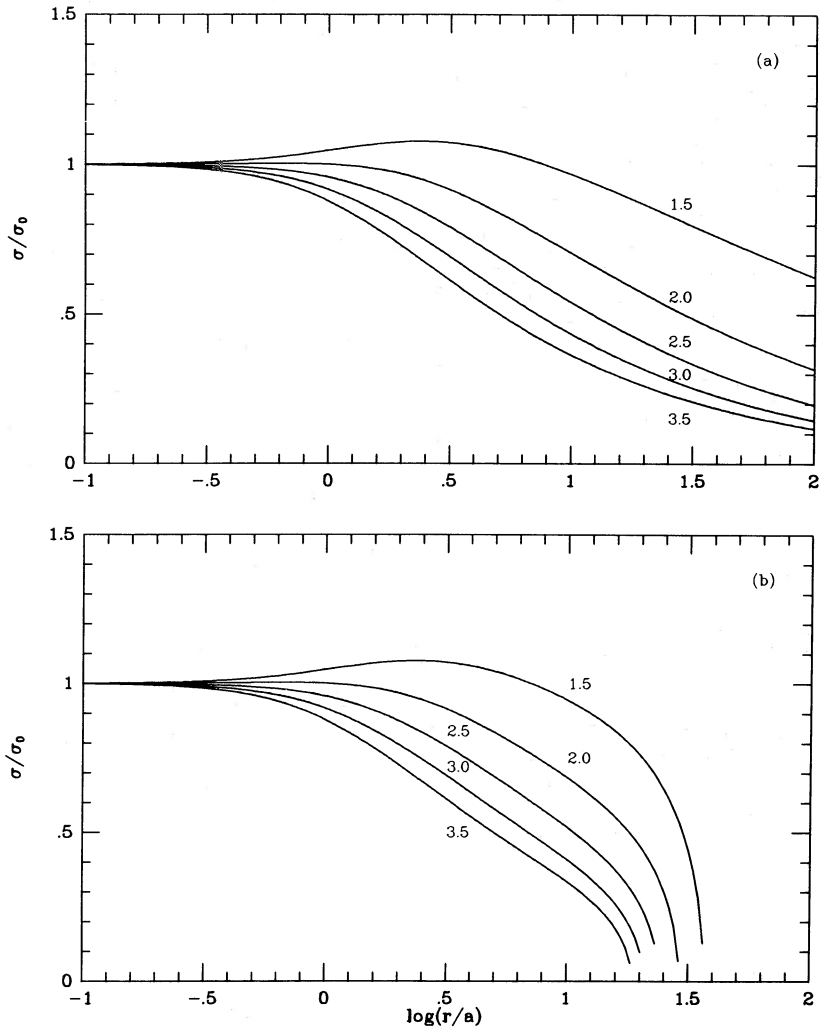

FIG. 14.—One-dimensional velocity dispersion as a function of radius from eq. (16) with the values of γ indicated, for (*a*) an isolated cluster and (*b*) a cluster in a tidal field with $(4\Omega^2 - \kappa^2)/G\rho_0 = 3.8 \times 10^{-4}$.

where r_h is the median radius of a cluster, i.e., the radius containing half the mass in three dimensions; the values of r_h are listed in Table 5. The local time scale for two-body relaxation may be calculated from (Spitzer and Hart 1971)

$$\tau_r(r) = \frac{0.147\sigma^3(r)}{G^2\langle m\rangle\rho(r)\log_{10}\Lambda}, \quad (19)$$

where $\langle m\rangle$ is the mean stellar mass. Finally, the reference relaxation time defined by Spitzer and Hart (1971) follows from equation (19) and the virial theorem:

$$\tau_{rh} = \frac{0.060M^{1/2}r_h^{3/2}}{G^{1/2}\langle m\rangle\log_{10}\Lambda}. \quad (20)$$

This is the relaxation time at the mean density within r_h. We adopt $\Lambda = 0.15M/\langle m\rangle$ for the Coulomb factor (Henon 1973); the exact value has little effect on the results. For a reasonable range of IMF slopes and upper and lower cutoffs, we estimate $0.2 \lesssim \langle m\rangle/M_\odot \lesssim 1.0$, and as a compromise, we adopt $\langle m\rangle = 0.5\ M_\odot$. The crossing times, and the central and reference relaxation times for the clusters in our sample, are listed in Table 2.

With Hodge's estimates of the ages, all the clusters are much younger than their central relaxation times. With Chiosi's estimates, about half the clusters are younger than their central relaxation times; the other half have $\tau_r(r) < \tau$ only at $r \lesssim a$. The densities in the regions where the star counts were made are so low that even the most massive stars are still not relaxed. Thus, if there is mass segregation in NGC 1866, it must be primordial. With either set of ages the clusters are older than their crossing times. Thus, allowing for the uncertainties in the ages and time scales, all the clusters in our sample are probably well mixed but not relaxed by two-body encounters, except perhaps within some of the cores. These conclusions are not altered by a distance modulus of 18.2 because $\tau_r(0)/\tau$ and τ_{rh}/τ would decrease by only 50% and $\tau_c(r_h)/\tau$ would decrease by only 40%.

VI. DISCUSSION

a) Cluster Formation

The rich star clusters in the Magellanic Clouds provide a valuable opportunity to study processes that may be relevant to the formation and early evolution of globular-like clusters. One intriguing property of the clusters in our sample is that they have spatial density profiles that fall off as power laws

with indices $\gamma + 1 \approx 3.5$. We now consider what this may imply about the progenitors of the clusters.

The three parameters most likely to affect the initial structure of a star cluster are the efficiency and time scale of star formation and the degree of clumpiness in the progenitor cloud. The efficiency is defined here as the ratio of the mass in the final star cluster to the mass in the initial gas cloud. Star formation may be either "fast" or "slow," depending on whether it is completed on a time scale shorter or longer than the crossing time in a protocluster. We assume that star formation continues until all the gas is used up or removed from a protocluster. If the initial motions of the stars reflect the turbulent motions of the gas from which they formed, then the crossing time in the protocluster will be comparable to that of the resulting stellar system (see eq. [18]). Fast star formation is probably unrealistic because it requires that all activity within a protocluster be synchronized on a time scale shorter than the crossing time. However, it does allow a purely stellar dynamical treatment that can be studied by N-body simulations. Slow star formation is probably more realistic, but the outcome is harder to predict.

From the small scatter in the luminosities of the blue giants in seven LMC clusters, including four in our sample, Robertson (1974*b*) finds age spreads $\lesssim 10^7$ yr. In Galactic open clusters the age spreads are typically $\sim 10^7$ yr (Herbst and Miller 1982; Stahler 1985 and references therein). Emission nebulosity is observed in many of the LMC clusters with ages $\lesssim 10^7$ yr; this gives some indication of the time scale for the removal of gas, and hence the time scale for star formation. For the clusters in our sample, the crossing times are $\sim 10^6$–10^7 yr. Thus the observations probably favor slow star formation, but fast star formation cannot be ruled out.

If star formation is fast, and the efficiency is *low*, a protocluster may lose more than 50% of its mass on a time scale shorter than the crossing time, in which case it cannot remain bound (Elmegreen 1983; Mathieu 1983; Lada, Margulis, and Dearborn 1984). On the other hand, if star formation is fast and the efficiency is *high*, the resulting stellar system will evolve nondissipatively. Van Albada (1982) and McGlynn (1984) have studied the collapse and violent relaxation of stellar systems using N-body codes with large dynamic ranges. In all cases the systems collapse, reexpand past their original limits, and reach an equilibrium configuration after a few crossing times. The density profile of the final state is determined mainly by the initial virial ratio, $2T_0/W_0$. For $2.2 \lesssim \gamma \lesssim 3.2$, McGlynn's models, which are fitted by a function of the same form as equation (13a), imply $0.2 \lesssim 2T_0/W_0 \lesssim 0.5$. (Note that our parameters γ and a are $\gamma - 1$ and r_c in his notation.) Thus, if the LMC clusters formed without dissipation, the initial conditions must have been "warm." The median radii of the progenitor clouds would have been about twice those of the present clusters, or roughly 20–30 pc.

We now consider whether protoclusters with slow star formation might have density profiles like those observed in our sample. If the efficiency of star formation is *low*, so that a large amount of mass is lost on a time scale longer than the crossing time, then, in contrast to the case of fast star formation, the cluster will remain bound. The density profile may, however, change dramatically, and since the relative amount of gas lost from the inner and outer parts may vary between protoclusters, a large spread in the indices γ might be expected. The similarity of the observed profiles therefore suggests that the efficiency of star formation was relatively high.

If star formation is slow but the efficiency is *high*, then, under some conditions, a protocluster may evolve toward an $r^{-3.5}$ profile independent of the initial structure. In a purely stellar system, stars on elongated orbits suffer changes in energy through two-body encounters as they pass through the dense central regions. The rate at which stars diffuse outward is constant, and it can be shown that an $r^{-3.5}$ profile results on the time scale for two-body relaxation (Spitzer and Shapiro 1972; Shapiro and Lightman 1976). Because of the disparity between the ages and the relaxation times of the clusters in our sample, star-star encounters are not important. However, if a mainly gaseous protocluster were sufficiently clumpy, relaxation through star-clump or clump-clump encounters might lead to an $r^{-3.5}$ profile by an analogous process. Using equations (18) and (20) for the crossing time and two-body relaxation time, the constraint $\tau_{rh} < \tau_c(r_h)$ suggests that the masses of the individual clumps must be at least 1% of the mass of the protocluster. The exact conditions necessary for such a process to be effective require further investigation.

Eventually, high-resolution observations of the gas in the LMC may help to distinguish between the different pictures for the formation of clusters. McGee and Milton (1966) have surveyed the LMC at 21 cm, with a beam size corresponding to 230 pc, and present a list of 52 H I complexes with mean radius 300 pc, mean density $n_H \approx 1$ cm^{-3}, and mean mass 4×10^6 $M_\odot$. Current CO surveys with a beam size corresponding to 120 pc indicate that molecules are underabundant compared with the disk of our Galaxy (Cohen, Montani, and Rubio 1984). Unfortunately neither of these surveys has high enough resolution to detect structure on the scale of protoclusters. The H I complexes observed by McGee and Milton are probably too big to be the progenitors of even the richest clusters, and in fact they may be unbound in the tidal field of the LMC (Blitz and Glassgold 1982). It is interesting to note, however, that four of the clusters in our sample, NGC 2156, NGC 2159, NGC 2164, and NGC 2172, could have formed in a single H I complex. They are approximately coeval, their combined mass is $\sim 3 \times 10^5$ $M_\odot$, and they occupy a region 375 pc $\times$ 270 pc.

b) Tidal Truncation and Unbound Halos

Perhaps the most intriguing feature of the clusters in our sample is that they do not appear to be tidally truncated. An unbound "halo" would be expected if expansion due to mass loss or violent relaxation caused a protocluster to spill over its Roche limit. The unbound stars may require several orbits to find the holes in the equipotential surfaces, and thus would be stripped by the tidal field on a time scale of several orbital periods of the cluster around the LMC. Since the clusters in our sample typically have completed only a tenth of an orbit, any unbound halos should still be intact. There is some evidence for an unbound halo around the Hyades (Pels, Oort, and Pels-Kluyver 1975). Furthermore, it has been proposed that the "moving groups" of stars in the disk of our Galaxy may be the result of the tidal stripping and eventual dissolution of star clusters (Eggen 1965, 1984; Woolley 1965).

We now estimate the eventual tidal radii of the clusters in our sample, and how much mass is present in the unbound halos. The tidal radius is usually taken as the inner Lagrangian point at the pericenter of the orbit around the parent galaxy:

$$r_t = \left(\frac{GM_t}{4\Omega^2 - \kappa^2} \right)^{1/3}, \qquad (21)$$

where M_t is the mass of the cluster (King 1962). This is consistent with equation (15), since the pressure gradient must vanish at the tidal radius. Keenan (1981*a*, *b*) integrates the restricted 3-body problem for clusters on circular and elliptical orbits around a galaxy, and argues for a tidal radius smaller by about 30%. However, on the basis of similar experiments, Seitzer (1983, 1985) finds that equation (21) is a good approximation. We adopt the larger radius because it gives more conservative estimates of the mass in unbound halos.

To estimate the eventual tidal radii of the clusters, we could simply integrate the observed profiles outward until equation (21) is satisfied. A more realistic approach might be to assume that unbound stars are stripped in such a way that the density profiles evolve toward King models with the same central properties as the clusters. This is valid if the core parameters do not change significantly during the time required for tidal truncation. The core of a cluster is expected to collapse on a time scale of 2–$10\tau_{rh}$, the exact coefficient depending on the stellar mass function and the number of binaries (Inagaki and Saslaw 1985 and references therein). Tidal stripping requires 5–10 orbital periods of the cluster around the parent galaxy (Keenan 1981*a*, *b*; Seitzer 1983, 1985). The values of τ_{rh} and τ_{orb} in Table 2 indicate that the time scale for core collapse is $\sim 10^{10}$ yr, while the time scale for truncation is $\sim 10^9$ yr. Thus we expect the clusters in our sample to be tidally truncated before their cores evolve significantly.

The core radius of a centrally concentrated cluster is related to the parameter a by

$$r_c \approx a(2^{2/\gamma} - 1)^{1/2} . \tag{22}$$

The total mass of a King model may be expressed in the form

$$M_t = \rho_0 r_c^3 g(c) , \tag{23}$$

where $c \equiv \log (r_t/r_c)$ is the concentration parameter and $g(c)$ is a dimensionless function. Using equations (21) and (23), we may solve for r_t, given r_c and ρ_0. The corresponding King (1962) models are plotted as the dashed curves in the lower panels (*b*) of Figures 1–10, and the core and tidal radii are listed in Table 5. The two curves represent extreme upper and lower limits, from the uncertainties in the mass-to-light ratios and the tidal field of the LMC. The inferred concentration parameters lie in the range $1.0 \lesssim c \lesssim 2.0$, which may be compared with the observed range $0.8 \lesssim c \lesssim 2.5$ for Galactic globular clusters (Webbink 1985) and the observed values $c = 1.1$, 1.4, and 1.5 for three old LMC clusters (Elson and Freeman 1985).

Irrespective of the future evolution of the clusters, the dashed curves in the lower panels (*b*) of Figures 1–10 are close to King models that fit the aperture photometry and are tidally limited by the LMC. In all cases, the star counts extend well beyond the lower limit on the tidal radius, and in a few cases they extend beyond the upper limit. Therefore, unless the mass-to-light ratios are all near the maximum possible values, at least some and perhaps all the clusters in our sample have unbound halos. The masses of the halos range up to 50% of M_∞. This result is essentially independent of the distance to the LMC because r_t and r_{max} scale in nearly the same way. For the smaller tidal radii preferred by Keenan (1981*a*, *b*), the evidence for unbound halos is strengthened. The uncertainties in the tidal limits could be reduced considerably by determining the IMF slopes and velocity dispersions within the clusters. We plan to report on such studies in future papers.

We are grateful to Ray Carlberg, Garth Illingworth, Neil Killeen, Robert Lupton, and Don Schneider for helpful suggestions during the course of this work, and to Joanne Fisher for help with the star counts. We also thank Bob Mathieu, the referee, for valuable comments on the manuscript. R. A. W. E. is supported by an Isaac Newton Studentship from the University of Cambridge, by a grant from the Corning Glass Works Foundation, and by National Science Foundation grant PHY-8217352.

TABLE 6

APERTURE PHOTOMETRY

Cluster (NGC) (1)	V (2)	$B-V$ (3)	d (4)	References (5)
1818	12.41	0.23	8	1
	11.80	0.14	11	1
	10.98	0.16	18	1
	10.28	0.18	29	1
	9.98	0.18	45	1
	9.70	0.18	72	1
	9.85	0.18	60	2
1831	11.18	0.34	60	2
	11.85	0.33	32	3
	11.38	0.39	48	3
	10.92	0.32	71	3
	10.66	0.33	110	3
	14.30	...	8.4	3
	13.84	...	12.4	3
	12.82	...	18.8	3
	12.29	...	28	3
	11.57	...	42	3
	11.11	...	62	3
	10.72	...	92	3
	10.44	...	137	3
	13.03	...	18.8	3
	12.12	...	28	3
	11.54	...	42	3
	11.06	...	63	3
	10.76	...	93	3
	10.46	...	142	3
	10.23	...	204	3
	11.09	0.29	62	3
1866	13.47	0.23	8	1
	12.49	0.27	11	1
	11.65	0.27	18	1
	10.73	0.26	29	1
	10.15	0.25	45	1
	9.73	0.25	72	1
	9.89	0.26	60	2
	10.59	0.27	32	3
	9.69	0.23	71	3
	9.45	0.22	110	3
	12.81	...	8.4	3
	12.15	...	12.4	3
	11.35	...	18.8	3
	10.74	...	28	3
	10.17	...	42	3
	9.77	...	62	3
	9.48	...	92	3
	9.21	...	137	3
	9.76	0.24	62	3
2004	11.76	0.18	8	1
	11.04	0.26	11	1
	10.59	0.24	18	1
	10.16	0.17	29	1
	9.95	0.11	45	1
	9.60	0.13	72	1
	9.86	0.11	60	2
2156	11.38	0.12	72	1
	12.44	0.15	13.3	4
	12.30	0.10	15.7	4
	11.88	0.09	25.4	4
	11.59	0.06	39.9	4
	11.38	0.07	55.2	4
	11.24	0.07	78.7	4
	11.09	0.06	112.0	4
2157	10.16	0.19	60	2
	12.00	0.17	13.3	4
	11.46	0.19	15.7	4
	10.82	0.17	25.4	4
	10.36	0.17	39.9	4
	10.13	0.19	55.2	4
	10.01	0.18	78.7	4
	9.92	0.18	112.0	4
2159	11.38	0.28	72	1
	12.94	0.15	15.7	4
	12.38	0.14	25.4	4
	11.86	0.21	39.9	4
	11.50	0.23	55.2	4
	11.39	0.21	78.7	4
	11.31	0.20	112.0	4
2164	10.34	0.10	60	2
	11.74	0.05	13.3	4
	11.54	0.05	15.7	4
	10.96	0.05	25.4	4
	10.58	0.09	39.9	4
	10.38	0.09	55.2	4
	10.17	0.11	78.7	4
	10.08	0.11	112.0	4
2172	11.75	0.18	72	1
	13.28	0.14	15.7	4
	12.37	0.20	25.4	4
	12.06	0.19	39.9	4
	11.85	0.16	55.2	4
	11.71	0.17	78.7	4
	11.60	0.16	112.0	4
2214	10.93	0.11	60	2
	12.88	0.12	13.3	4
	12.54	0.06	15.7	4
	11.87	0.06	25.4	4
	11.36	0.05	39.9	4
	10.95	0.10	55.2	4
	10.69	0.10	78.7	4
	10.53	0.14	112.0	4

Col. (1).—Cluster name.
Col. (2).—V-magnitude, not corrected for absorption.
Col. (3).—$B-V$ color from the aperture photometry.
Col. (4).—Aperture diameter in arcsec.
REFERENCES.—(1) Bernard and Bigay 1974; (2) van den Bergh and Hagen 1968; (3) Gordon and Kron 1983; (4) this paper.

TABLE 7

STAR COUNTS

A. NGC 1818

PLATE AAT − (△) $s = 16''.4\ mm^{-1}$ $d = 60$ mm $\log A = -3.16$		PLATE 1004 (●) $s = 16''.4\ mm^{-1}$ $d = 60$ mm $\log A = -3.12$		PLATE 1045 (○) $s = 16''.4\ mm^{-1}$ $d = 60$ mm $\log A = -3.49$		PLATE 1337 (▲) $s = 16''.4\ mm^{-1}$ $d = 60$ mm $\log A = -3.16$	
r	$\log f_c$	r	$\log f_c$	r	$\log f_c$	r	$\log f_c$
0'.55–0'.82	1.63(0.06)	0'.55–0'.82	1.84(0.19)	0'.55–0'.82	1.93(0.04)	0'.55–0'.82	1.72(0.16)
0.82–1.09	1.54(0.03)	0.82–1.09	1.65(0.15)	0.82–1.09	1.74(0.01)	0.82–1.09	1.63(0.14)
1.09–1.37	1.24	1.09–1.37	1.47(0.11)	1.09–1.37	1.43	1.09–1.37	1.22(0.08)
1.37–1.64	1.10	1.37–1.64	1.08(0.06)	1.37–1.64	1.17	1.37–1.64	0.99(0.06)
1.64–1.91	0.89	1.64–1.91	0.93(0.05)	1.64–1.91	0.98	1.64–1.91	0.51(0.04)
1.91–2.19	0.20	1.91–2.19	0.73(0.04)	1.91–2.19	0.85	1.91–2.19	0.01(0.03)
2.19–2.46	0.48	2.19–2.46	0.70(0.04)	2.19–2.46	0.91	2.19–2.46	0.04(0.03)
2.46–2.73	0.52	2.46–2.73	−0.34(0.02)	2.46–2.73	0.37	$\log f_b$	1.69(0.03)
2.73–3.01	−0.56	2.73–3.01	0.74(0.04)	2.73–3.01	0.54	$\log f_0$	−0.78
3.01–3.28	0.67	3.01–3.28	−0.41(0.02)	3.01–3.28	0.56		
$\log f_b$	1.20	$\log f_b$	1.64(0.02)	3.28–3.55	0.66		
$\log f_0$	−0.64	$\log f_0$	−0.93	$\log f_b$	1.49		
				$\log f_0$	−0.88		

B. NGC 1831

PLATE 1035 (●) $s = 16''.4\ mm^{-1}$ $d = 60$ mm $\log A = -2.91$		PLATE 1036 (■) $s = 16''.4\ mm^{-1}$ $d = 60$ mm $\log A = -2.91$		PLATE 1046 (▲) $s = 16''.4\ mm^{-1}$ $d = 60$ mm $\log A = -2.92$	
r	$\log f_c$	r	$\log f_c$	r	$\log f_c$
0'.82–1'.09	2.04(0.33)	0'.55–0'.82	2.20(0.37)	0'.55–0'.82	2.22(0.37)
1.09–1.37	1.83(0.27)	0.82–1.09	2.01(0.30)	0.82–1.09	2.00(0.28)
1.37–1.64	1.63(0.22)	1.09–1.37	1.82(0.24)	1.09–1.37	1.79(0.21)
1.64–1.91	1.46(0.18)	1.37–1.64	1.53(0.16)	1.37–1.64	1.56(0.14)
1.91–2.19	1.21(0.14)	1.64–1.91	1.35(0.12)	1.64–1.91	1.37(0.08)
2.19–2.46	1.07(0.13)	1.91–2.19	1.20(0.09)	1.91–2.19	1.09(0.02)
2.46–2.73	1.07(0.13)	2.19–2.46	1.02(0.07)	2.19–2.46	0.88
2.73–3.01	0.79(0.11)	2.46–2.73	0.95(0.06)	2.46–2.73	0.64
3.01–3.28	−0.10(0.08)	2.73–3.01	0.60(0.03)	2.73–3.01	0.61
3.28–3.55	0.24(0.08)	3.01–3.28	0.73(0.04)	3.01–3.28	0.93
3.55–3.83	0.84(0.11)	3.28–3.55	0.10(0.01)	3.28–3.55	−0.49
3.83–4.10	−0.64(0.08)	3.55–3.83	0.34(0.02)	3.55–3.83	0.49
4.10–4.37	−0.23(0.08)	$\log f_b$	1.39(0.01)	3.83–4.10	0.31
4.37–4.65	0.45(0.09)	$\log f_0$	−1.69	4.10–4.37	0.15
$\log f_b$	1.57(0.08)			$\log f_b$	1.21
$\log f_0$	−1.82			$\log f_0$	−1.65

PLATE 1280 (△) $s = 25''.0\ mm^{-1}$ $d = 45$ mm $\log A = -3.14$		PLATE 1047 (□) $s = 16''.4\ mm^{-1}$ $d = 90$ mm $\log A = -3.07$		PLATE 3764 (○) $s = 25''.0\ mm^{-1}$ $d = 45$ mm $\log A = -3.09$		PLATE 1279 (×) $s = 25''.0\ mm^{-1}$ $d = 45$ mm $\log A = -3.14$	
r	$\log f_c$	r	$\log f_c$	r	$\log f_c$	r	$\log f_c$
0'.31–0'.63	2.19(0.28)	0'.41–0'.82	2.00(0.20)	0'.63–0'.94	1.91(0.19)	0'.63–0'.94	1.67(0.06)
0.63–0.94	1.90(0.16)	0.82–1.23	1.66(0.07)	0.94–1.25	1.72(0.12)	0.94–1.25	1.22
0.94–1.25	1.64(0.06)	1.23–1.64	1.28	1.25–1.56	1.46(0.02)	1.25–1.56	0.78
1.25–1.56	1.21	1.64–2.05	0.90	1.56–1.88	1.11	1.56–1.88	0.38
1.56–1.88	1.10	2.05–2.46	0.67	1.88–2.19	0.90	1.88–2.19	−0.05
1.88–2.19	0.79	2.46–2.87	0.43	2.19–2.50	0.37	$\log f_b$	0.38
2.19–2.50	0.04	2.87–3.28	0.45	2.50–2.81	0.60	$\log f_0$	−0.82
2.50–2.81	−0.06	3.28–3.69	−0.18	2.81–3.13	0.51		
2.81–3.13	0.71	3.69–4.10	0.06	3.13–3.44	0.71		
3.13–3.44	0.42	4.10–4.51	−0.13	3.44–3.75	0.11		
3.44–3.75	0.07	4.51–4.92	0.11	3.75–4.06	0.32		
$\log f_b$	0.59	$\log f_b$	0.78	4.06–4.38	−0.13		
$\log f_0$	−1.19	$\log f_0$	−1.20	4.38–4.69	0.20		
				4.69–5.00	0.41		
				$\log f_b$	0.91		
				$\log f_0$	−1.32		

TABLE 7—*Continued*

C. NGC 1866

PLATE 529 (●) $s = 16''.4\ mm^{-1}$ $d = 90$ mm $\log A = -2.95$		PLATE 878 (○) $s = 25''.0\ mm^{-1}$ $d = 60$ mm $\log A = -3.31$		PLATE 1049 (▲) $s = 16''.4\ mm^{-1}$ $d = 90$ mm $\log A = -2.78$		PLATE 1050 (*) $s = 16''.4\ mm^{-1}$ $d = 90$ mm $\log A = -2.83$		PLATE 1051 (△) $s = 16''.4\ mm^{-1}$ $d = 90$ mm $\log A = -2.86$	
r	$\log f_c$	r	$\log f_c$	r	$\log f_c$	r	$\log f_c$	r	$\log f_c$
0.82–1.23	1.78(0.28)	0.83–1.25	1.66	0.41–0.82	1.98(0.33)	1.41–0.82	1.81(0.22)	0.41–0.82	1.71(0.16)
1.23–1.64	1.65(0.25)	1.25–1.67	1.43	0.82–1.23	1.65(0.21)	0.82–1.23	1.34(0.03)	0.82–1.23	1.25
1.64–2.05	1.52(0.23)	1.67–2.08	1.14	1.23–1.64	1.44(0.14)	1.23–1.64	1.09	1.23–1.64	0.58
2.05–2.46	1.43(0.22)	2.08–2.50	0.90	1.64–2.05	1.19(0.07)	1.64–2.05	0.81	1.64–2.05	0.35
2.46–2.87	1.09(0.18)	2.50–2.92	0.63	2.05–2.46	1.02(0.03)	2.05–2.46	0.62	2.05–2.46	0.45
2.87–3.28	0.89(0.17)	2.92–3.33	0.43	2.46–2.87	0.85	2.46–2.87	0.29	2.46–2.87	−0.16
3.28–3.69	0.69(0.16)	3.33–3.75	0.64	2.87–3.28	0.52	2.87–3.28	0.29	2.87–3.28	0.08
3.69–4.10	0.27(0.16)	3.75–4.17	0.19	3.28–3.69	0.75	3.28–3.69	0.38	3.28–3.69	0.00
4.10–4.51	0.68(0.16)	4.17–4.58	0.01	3.69–4.10	0.58	3.69–4.10	0.18	3.69–4.10	0.00
4.51–4.92	0.79(0.17)	4.58–5.00	0.19	4.10–4.51	0.59	4.10–4.51	−0.25	$\log f_b$	0.13
4.92–5.33	−0.36(0.15)	5.00–5.42	0.24	4.51–4.92	0.42	4.51–4.92	0.10	$\log f_0$	−0.21
5.33–5.74	0.41(0.16)	5.42–5.83	0.16	4.92–5.33	0.18	4.92–5.33	−0.07		
5.74–6.15	0.68(0.16)	5.83–6.25	−1.16	5.33–5.74	0.15	5.33–5.74	−0.11		
6.15–6.56	0.75(0.17)	$\log f_b$	0.50	5.74–6.15	0.25	5.74–6.15	−0.07		
6.56–6.97	0.24(0.15)	$\log f_0$	−0.72	6.15–6.56	0.17	$\log f_b$	0.46		
6.97–7.38	0.51(0.16)			6.56–6.97	0.33	$\log f_0$	−0.46		
7.38–7.79	0.47(0.16)			6.97–7.38	0.13				
7.79–8.20	−0.10(0.15)			7.38–7.79	0.16				
8.20–8.61	0.53(0.15)			7.79–8.20	0.10				
$\log f_b$	1.78(0.15)			8.20–8.61	0.16				
$\log f_0$	−1.18			8.61–9.02	−0.04				
				$\log f_b$	1.04				
				$\log f_0$	−0.86				

PLATE 2108 (□) $s = 25''.0\ mm^{-1}$ $d = 60$ mm $\log A = -3.46$		PLATE 2251 (*) $s = 11''.3\ mm^{-1}$ $d = 60$ mm $\log A = -3.67$		PLATE 3467 (■) $s = 25''.0\ mm^{-1}$ $d = 60$ mm $\log A = -3.07$	
r	$\log f_c$	r	$\log f_c$	r	$\log f_c$
0.42–0.83	1.97(0.04)	0.00–0.19	2.70(0.21)	0.83–1.25	1.83(0.21)
0.83–1.25	1.40	0.19–0.38	2.44(0.10)	1.25–1.67	1.76(0.19)
1.25–1.67	1.03	0.38–0.56	2.26(0.03)	1.67–2.08	1.45(0.10)
1.67–2.08	0.55	0.56–0.75	2.03	2.08–2.50	1.30(0.07)
2.08–2.50	0.46	0.75–0.94	1.61	2.50–2.92	1.07(0.03)
2.50–2.92	0.24	0.94–1.13	1.39	2.92–3.33	0.72
2.92–3.33	−0.05	1.13–1.32	1.19	3.33–3.75	0.74
3.33–3.75	0.16	1.32–1.51	0.92	3.75–4.17	0.61
$\log f_b$	−0.03	1.51–1.70	0.77	4.17–4.58	0.77
$\log f_0$	−0.41	1.70–1.88	0.81	4.58–5.00	0.41
		1.88–2.07	0.81	5.00–5.42	0.30
		2.07–2.26	0.80	5.42–5.83	0.07
		2.26–2.45	0.53	5.83–6.25	0.01
		2.45–2.64	0.47	6.25–6.67	0.22
		2.64–2.83	0.11	6.67–7.08	0.16
		2.83–3.01	0.59	7.08–7.50	−0.16
		3.01–3.20	0.33	7.50–7.92	0.60
		3.20–3.39	0.59	7.92–8.33	0.31
		3.39–3.58	0.19	$\log f_b$	1.39
		3.58–3.77	0.19	$\log f_0$	−1.13
		3.77–3.95	0.25		
		$\log f_b$	0.48		
		$\log f_0$	−0.45		

TABLE 7—*Continued*

D. NGC 2004

PLATE 1345 (■) $s = 16''.4$ mm^{-1} $d = 60$ mm $\log A = -3.31$		PLATE 1346 (▲) $s = 16''.4$ mm^{-1} $d = 60$ mm $\log A = -3.36$	
r	$\log f_c$	r	$\log f_c$
0'.55–0'.82	1.84(0.18)	0'.27–0'.55	2.20(0.21)
0.82–1.09	1.56(0.14)	0.55–0.82	1.82(0.11)
1.09–1.37	1.38(0.12)	0.82–1.09	1.65(0.07)
1.37–1.64	0.98(0.09)	1.09–1.37	1.48(0.04)
1.64–1.91	0.97(0.09)	1.37–1.64	1.19(0.01)
1.91–2.19	0.88(0.09)	1.64–1.91	1.18(0.01)
2.19–2.46	0.82(0.09)	1.91–2.19	0.95
2.46–2.73	0.48(0.08)	2.19–2.46	1.16
2.73–3.01	0.53(0.08)	2.46–2.73	0.73
3.01–3.28	0.80(0.09)	2.73–3.01	0.87
$\log f_b$	1.97(0.08)	3.01–3.28	0.71
$\log f_0$	−0.85	3.28–3.55	−0.61
		3.55–3.83	−0.21
		$\log f_b$	1.78
		$\log f_0$	−0.81

E. NGC 2156

PLATE 539 (■) $s = 15''.2$ mm^{-1} $d = 90$ mm $\log A = -2.78$		PLATE 1258 (×) $s = 25''.0$ mm^{-1} $d = 45$ mm $\log A = -3.14$		PLATE 1266 (*) $s = 25''.0$ mm^{-1} $d = 45$ mm $\log A = -2.81$		PLATE 1338 (●) $s = 16''.4$ mm^{-1} $d = 60$ mm $\log A = -3.45$	
r	$\log f_c$	r	$\log f_c$	r	$\log f_c$	r	$\log f_c$
0'.38–0'.76	1.69(0.29)	0'.31–0'.63	0.62	0'.31–0'.63	1.34(0.06)	0'.55–0'.82	1.79(0.06)
0.76–1.14	1.45(0.24)	0.63–0.94	0.38	0.63–0.94	0.79	0.82–1.09	1.46
1.14–1.52	1.02(0.18)	0.94–1.25	0.08	0.94–1.25	0.44	1.09–1.37	1.12
1.90–2.28	0.18(0.15)	1.25–1.56	−0.76	1.25–1.56	−0.90	1.37–1.64	0.95
2.28–2.66	0.35(0.15)	1.56–1.88	−0.39	1.56–1.88	0.36	1.64–1.91	0.46
2.66–3.04	−0.36(0.14)	1.88–2.19	−0.09	1.88–2.19	−0.53	1.91–2.19	0.42
3.04–3.42	0.28(0.15)	$\log f_b$	−0.71	2.19–2.50	−0.25	$\log f_b$	1.72
3.42–3.80	0.47(0.15)	$\log f_0$	0.03	2.50–2.81	−0.72	$\log f_0$	−1.55
$\log f_b$	1.59(0.14)			2.81–3.13	−0.39		
$\log f_0$	−1.49			3.13–3.44	−0.36		
				3.44–3.75	−0.51		
				$\log f_b$	−0.02		
				$\log f_0$	−0.62		

PLATE 1339 (▲) $s = 16''.4$ mm^{-1} $d = 60$ mm $\log A = -2.94$		PLATE 1424 (□) $s = 25''.0$ mm^{-1} $d = 45$ mm $\log A = -3.55$		PLATE 1729 (△) $s = 25''.0$ mm^{-1} $d = 45$ mm $\log A = -3.63$		PLATE 3468 (○) $s = 25''.0$ mm^{-1} $d = 45$ mm $\log A = -2.84$	
r	$\log f_c$	r	$\log f_c$	r	$\log f_c$	r	$\log f_c$
0'.55–0'.82	1.66(0.19)	0'.31–0'.63	1.76	0'.31–0'.63	1.53	0'.31–0'.63	1.74(0.25)
0.82–1.09	1.43(0.14)	0.63–0.94	1.12	0.63–0.94	1.08	0.63–0.94	1.51(0.18)
1.09–1.37	1.15(0.09)	0.94–1.25	0.77	0.94–1.25	0.84	0.94–1.25	1.06(0.07)
1.37–1.64	0.75(0.05)	1.25–1.56	0.59	1.25–1.56	−0.13	1.25–1.56	0.57
1.64–1.91	0.60(0.04)	1.56–1.88	0.24	1.56–1.88	0.20	1.56–1.88	−0.11
1.91–2.19	1.30(0.11)	1.88–2.19	0.24	2.50–2.81	−0.02	$\log f_b$	1.15
2.19–2.46	0.60(0.04)	2.50–2.81	0.20	2.81–3.13	0.20	$\log f_0$	−1.30
$\log f_b$	1.45(0.02)	2.81–3.13	−0.24	3.13–3.44	−0.42		
$\log f_0$	−1.54	$\log f_b$	0.48	$\log f_b$	0.45		
		$\log f_0$	−1.02	$\log f_0$	−0.79		

TABLE 7—*Continued*

F NGC 2157

PLATE 544 (▲) $s = 15''.2$ mm^{-1} $d = 90$ mm log $A = -2.95$		PLATE 1347 (●) $s = 16''.4$ mm^{-1} $d = 60$ mm log $A = -3.55$		PLATE 1348 (■) $s = 16''.4$ mm^{-1} $d = 60$ mm log $A = -3.71$		PLATE 1349 (○) $s = 16''.4$ mm^{-1} $d = 45$ mm log $A = -3.30$	
r	log f_c	r	log f_c	r	log f_c	r	log f_c
0.'76–1.'14	1.71(0.22)	0.'55–0.'82	2.23(0.17)	0.'55–0.'82	2.20(0.07)	0.'41–0.'62	2.15(0.20)
1.14–1.52	1.38(0.15)	0.82–1.09	1.84(0.08)	0.82–1.09	1.85	0.62–0.82	1.76(0.07)
1.52–1.90	1.16(0.12)	1.09–1.37	1.62(0.05)	1.09–1.37	1.61	0.82–1.02	1.54(0.02)
1.90–2.28	0.73(0.08)	1.37–1.64	1.35(0.02)	1.37–1.64	1.31	1.02–1.23	1.26
2.28–2.66	0.91(0.09)	1.64–1.91	1.20(0.01)	1.64–1.91	1.21	1.23–1.43	0.95
2.66–3.04	0.30(0.07)	1.91–2.19	1.06	1.91–2.19	0.95	1.43–1.64	1.07
3.04–3.42	0.50(0.07)	2.19–2.46	0.08	2.46–2.73	0.68	1.64–1.85	0.67
3.42–3.80	0.15(0.07)	2.46–273	0.97	2.73–3.01	0.70	1.85–2.05	0.76
3.80–4.18	0.81(0.09)	2.73–3.01	0.93	3.01–3.28	0.70	2.05–2.25	0.56
4.18–4.56	0.16(0.07)	3.01–3.28	0.81	3.28–3.55	1.06	2.25–246	0.76
log f_b	1.58(0.06)	3.28–3.55	0.74	log f_b	1.80	2.46–2.66	0.65
log f_0	−1.48	log f_b	1.98	log f_0	−1.42	log f_b	1.50
		log f_0	−1.53			log f_0	−1.08

PLATE 1854 (□) $s = 25''.0$ mm^{-1} $d = 45$ mm log $A = -2.77$		PLATE 1965 (×) $s = 11''.3$ mm^{-1} $d = 45$ mm log $A = -3.47$		PLATE 1975 (△) $s = 25''.0$ mm^{-1} $d = 45$ mm log $A = -3.38$	
r	log f_c	r	log f_c	r	log f_c
0.'31–0.'63	1.49(0.16)	0.'00–0.'14	2.72(0.31)	0.'31–0.'63	1.81(0.02)
0.63–0.94	1.16(0.04)	0.14–0.28	2.37(0.15)	0.63–0.94	1.43
0.94–1.25	0.84	0.28–0.42	1.64	0.94–1.25	0.97
1.25–1.56	0.70	0.42–0.56	1.55	1.25–1.56	0.97
1.56–1.88	0.53	0.56–0.71	1.44	1.56–1.88	0.57
1.88–2.19	−0.08	0.71–0.85	0.89	1.88–2.19	0.26
2.19–2.50	0.19	0.85–0.99	0.72	2.19–2.50	0.23
log f_b	0.72	0.99–1.13	0.88	2.50–2.81	−0.33
log f_0	−0.43	1.13–1.27	0.67	log f_b	0.74
		1.27–1.41	0.61	log f_0	−0.63
		1.41–1.55	0.33		
		1.55–1.70	0.06		
		1.70–1.84	0.46		
		1.84–1.98	−0.07		
		1.98–2.12	−0.14		
		2.12–2.26	−0.21		
		2.26–2.40	−0.30		
		2.40–2.54	−0.35		
		log f_b	−0.04		
		log f_0	−0.30		

G. NGC 2159

PLATE 539 (■) $s = 15''.2$ mm^{-1} $d = 90$ mm log $A = -2.78$		PLATE 1266 (*) $s = 25''.0$ mm^{-1} $d = 45$ mm log $A = -2.81$		PLATE 1338 (●) $s = 16''.4$ mm^{-1} $d = 60$ mm log $A = -3.45$	
r	log f_c	r	log f_c	r	log f_c
0.'38–0.'76	1.73(0.30)	0.'00–0.'31	1.68(0.20)	0.'55–0.'82	1.70(0.03)
0.76–1.14	1.39(0.23)	0.31–0.63	1.16	0.82–1.09	1.56(0.01)
1.14–1.52	1.21(0.21)	0.63–0.94	−0.26	1.09–1.37	1.31
1.90–2.28	0.31(0.16)	0.94–1.25	0.59	1.37–1.64	1.21
2.28–2.66	0.14(0.15)	1.25–1.56	0.40	1.91–2.19	0.60
log f_b	1.61(0.15)	1.56–1.88	−0.86	2.19–2.46	0.72
log f_0	−1.35	1.88–2.19	−0.12	2.46–2.73	−0.31
		log f_b	−0.13	2.73–3.01	0.76
		log f_0	−0.33	3.01–3.28	0.51
				3.28–3.55	0.29
				3.55–3.83	0.71
				3.83–4.10	0.68
				log f_b	1.71
				log f_0	−1.25

TABLE 7—*Continued*

G. NGC 2159—*Continued*

PLATE 1339 (▲) $s = 16''.4\ mm^{-1}$ $d = 60$ mm $\log A = -2.94$		PLATE 1424 (□) $s = 25''.0\ mm^{-1}$ $d = 45$ mm $\log A = -3.55$		PLATE 1729 (△) $s = 25''.0\ mm^{-1}$ $d = 45$ mm $\log A = -3.63$		PLATE 3468 (○) $s = 25''.0\ mm^{-1}$ $d = 45$ mm $\log A = -2.84$	
r	$\log f_c$	r	$\log f_c$	r	$\log f_c$	r	$\log f_c$
0'.55–0'.82	1.65(0.19)	0'.31–0'.63	1.65	0'.00–0'.31	1.81	0'.31–0'.63	1.71(0.24)
0.82–1.09	1.33(0.12)	0.63–0.94	1.05	0.31–0.63	1.08	0.63–0.94	1.28(0.11)
1.09–1.37	1.27(0.11)	0.94–1.25	0.43	0.63–0.94	0.91	0.94–1.25	0.77
1.37–1.64	1.08(0.08)	1.25–1.56	0.80	0.94–1.25	0.63	1.25–1.56	0.88
1.64–1.91	0.88(0.06)	1.56–1.88	0.41	1.25–1.56	0.16	1.56–1.86	0.43
1.91–2.19	0.82(0.05)	1.88–2.19	−0.09	1.56–1.88	0.36	$\log f_b$	1.10
2.19–2.46	0.67(0.04)	2.19–2.50	−0.09	1.88–2.19	−1.34	$\log f_0$	−0.95
2.46–2.73	0.62(0.04)	$\log f_b$	0.39	2.19–2.50	0.09		
2.73–3.01	0.84(0.05)	$\log f_0$	−0.66	$\log f_b$	0.48		
3.01–3.28	0.41(0.03)			$\log f_0$	−0.35		
3.28–3.55	0.68(0.04)						
3.55–3.83	0.43(0.03)						
3.83–4.10	0.45(0.03)						
$\log f_b$	1.44(0.02)						
$\log f_0$	−1.48						

H. NGC 2164

PLATE 539 (■) $s = 15''.2\ mm^{-1}$ $d = 90$ mm $\log A = -2.78$		PLATE 1258 (×) $s = 25''.0\ mm^{-1}$ $d = 45$ mm $\log A = -3.14$		PLATE 1266 (*) $s = 25''.0\ mm^{-1}$ $d = 45$ mm $\log A = -2.81$		PLATE 1388 (●) $s = 16''.4\ mm^{-1}$ $d = 60$ mm $\log A = -3.45$	
r	$\log f_c$	r	$\log f_c$	r	$\log f_c$	r	$\log f_c$
0'.76–1'.14	1.64(0.27)	0'.31–0'.63	0.80	0'.31—0'.63	1.42(0.09)	0'.55–0'.82	2.04(0.12)
1.14–1.52	1.41(0.22)	0.63–0.94	0.38	0.63–0.94	1.06	0.82–1.09	1.72(0.04)
1.52–1.90	1.09(0.18)	0.94–1.25	0.08	0.94–1.25	0.71	1.09–1.37	1.50
1.90–2.28	0.97(0.17)	1.25–1.56	−0.27	1.25–1.56	0.43	1.37–1.64	1.27
2.28–2.66	0.37(0.14)	1.56–1.88	−0.39	1.56–1.88	−0.29	1.64–1.91	1.18
2.66–3.04	0.74(0.15)	1.88–2.19	−1.20	1.88–2.19	0.11	1.91–2.19	1.01
3.04–3.42	0.23(0.13)	2.19–2.50	0.12	2.19–2.50	−0.25	2.19–2.46	0.63
3.42–3.80	0.18(0.13)	$\log f_b$	−0.72	2.50–2.81	−0.72	2.46–2.73	0.70
$\log f_b$	1.56(0.13)	$\log f_0$	0.35	$\log f_b$	−0.02	2.73–3.01	0.89
$\log f_0$	−1.48			$\log f_0$	−0.33	3.01–3.28	0.54
						3.28–3.55	0.46
						3.55–3.83	0.89
						3.83–4.10	0.43
						4.10–4.37	0.71
						$\log f_b$	1.74
						$\log f_0$	−1.33

PLATE 1339 (▲) $s = 16''.4\ mm^{-1}$ $d = 60$ mm $\log A = -2.94$		PLATE 1424 (□) $s = 25''.0\ mm^{-1}$ $d = 45$ mm $\log A = -3.55$		PLATE 1729 (△) $s = 25''.0\ mm^{-1}$ $d = 45$ mm $\log A = -3.63$		PLATE 3468 (○) $s = 25''.0\ mm^{-1}$ $d = 45$ mm $\log A = -2.84$	
r	$\log f_c$	r	$\log f_c$	r	$\log f_c$	r	$\log f_c$
0'.55–0'.82	1.83(0.24)	0'.31–0'.63	1.99(0.02)	0'.31–0'.63	1.81	0'.63–0'.94	1.63(0.21)
0.82–1.09	1.58(0.17)	0.63–0.94	1.49	0.63–0.94	1.33	0.94–1.25	1.33(0.13)
1.09–1.37	1.37(0.12)	0.94–1.25	0.96	0.94–1.25	0.89	1.25–1.56	1.00(0.05)
1.37–1.64	0.97(0.06)	1.25–1.56	0.72	1.25–1.56	0.66	1.56–1.88	0.78(0.02)
1.64–1.91	0.94(0.06)	1.56–1.88	0.20	1.56–1.88	0.24	1.88–2.19	0.69(0.01)
1.91–2.19	0.83(0.05)	1.88–2.19	0.41	1.88–2.19	0.31	2.19–2.50	0.19
2.19–2.46	0.25(0.02)	2.19–2.50	0.19	$\log f_b$	0.48	2.50–2.81	0.16
2.46–2.73	0.48(0.02)	2.50–2.81	0.06	$\log f_0$	−0.58	2.81–3.13	−0.28
2.73–3.01	0.65(0.03)	2.81–3.13	−0.84			3.13–3.44	0.38
3.01–3.28	0.14(0.01)	3.13–3.44	−0.13			3.44–3.75	0.43
3.28–3.55	0.34(0.02)	$\log f_b$	0.54			$\log f_b$	1.14
3.55–3.83	0.35(0.02)	$\log f_0$	−0.75			$\log f_0$	−1.13
$\log f_b$	1.43(0.01)						
$\log f_0$	−1.23						

TABLE 7—*Continued*

I. NGC 2172

PLATE 539 (■) $s = 15''.2$ mm^{-1} $d = 90$ mm log $A = -2.78$		PLATE 1266 (*) $s = 25''.0$ mm^{-1} $d = 45$ mm log $A = -2.81$		PLATE 1338 (●) $s = 16''.4$ mm^{-1} $d = 60$ mm log $A = -3.45$	
r	log f_c	r	log f_c	r	log f_c
0'.38–0'.76	1.67(0.28)	0'.00–0'.31	1.83(0.21)	0'.55–0'.82	1.47
0.76–1.14	1.09(0.18)	0.31–0.63	1.00	0.82–1.09	1.26
1.14–1.52	0.32(0.14)	0.63–0.94	0.79	1.09–1.37	1.07
1.52–1.90	0.10(0.13)	0.94–1.25	−0.05	1.37–1.64	1.03
1.90–2.28	−0.46(0.13)	log f_b	−0.02	1.64–1.91	0.81
log f_b	1.58(0.13)	log f_0	−0.54	1.91–2.19	0.73
log f_0	−1.54			log f_b	1.69
				log f_0	−1.39

PLATE 1424 (□) $s = 25''.0$ mm^{-1} $d = 45$ mm log $A = -3.55$		PLATE 1729 (△) $s = 25''.0$ mm^{-1} $d = 45$ mm log $A = -3.63$		PLATE 3468 (○) $s = 25''.0$ mm^{-1} $d = 45$ mm log $A = -2.84$	
r	log f_c	r	log f_c	r	log f_c
0'.00–0'.31	2.06(0.04)	0'.00–0'.31	2.11(0.03)	0'.31–0'.63	1.53(0.17)
0.31–0.63	1.46	0.31–0.63	1.31	0.63–0.94	1.01(0.03)
0.63–0.94	1.05	0.63–0.94	0.90	0.94–1.25	0.37
0.94–1.25	0.24	0.94–1.25	0.41	1.25–1.56	0.11
1.25–1.56	0.35	1.25–1.56	0.25	1.56–1.88	0.37
1.56–1.88	−0.10	1.56–1.88	0.00	1.88–2.19	0.05
1.88–2.19	0.12	1.88–2.19	0.16	log f_b	1.03
log f_b	0.39	log f_b	0.41	log f_0	−1.04
log f_0	−0.75	log f_0	−0.74		

J. NGC 2214

PLATE 533 (●) $s = 16''.4$ mm^{-1} $d = 90$ mm log $A = -3.11$		PLATE 3495 (▲) $s = 25''.0$ mm^{-1} $d = 60$ mm log $A = -2.95$		PLATE 3496 (○) $s = 25''.0$ mm^{-1} $d = 60$ mm log $A = -2.91$		PLATE 3497 (□) $s = 25''.0$ mm^{-1} $d = 60$ mm log $A = -2.94$	
r	log f_c	r	log f_c	r	log f_c	r	log f_c
0'.82–1'.23	1.71(0.16)	0'.42–0'.83	1.69(0.18)	0'.42–0'.83	1.78(0.21)	0'.42–0'.83	1.62(0.12)
1.23–1.64	1.37(0.09)	0.83–1.25	1.57(0.14)	0.83–1.25	1.48(0.09)	1.83–1.25	1.34(0.01)
1.64–2.05	1.11(0.06)	1.25–1.67	1.33(0.08)	1.25–1.67	1.20	1.25–1.67	0.96
2.05–2.46	0.91(0.04)	1.67–2.08	0.99	1.67–2.08	0.84	1.67–2.08	0.69
2.46–2.87	0.93(0.04)	2.08–2.50	0.73	2.08–2.50	0.62	2.08–2.92	0.34
2.87–4.51	0.00(0.01)	2.50–2.92	0.61	2.50–2.92	0.34	2.92–3.75	0.21
4.51–6.15	0.12(0.01)	2.92–3.75	0.15	2.92–4.58	0.15	3.75–4.58	−0.22
log f_b	1.61(0.01)	3.75–4.58	−0.02	4.58–6.25	−0.22	4.58–5.42	−0.19
log f_0	−1.36	4.58–5.42	−0.46	log f_b	0.68	log f_b	0.22
		log f_b	1.08	log f_0	−1.07	log f_0	−0.88
		log f_0	−1.08				

NOTE.—Plates identified with numbers greater than 1500 were taken with the 1 m telescope at Siding Spring Observatory, and the remaining plates were taken with the Anglo-Australian Telescope. Quantities given below each plate number are values of s, the plate scale in arcsec mm^{-1}; d, the reseau diameter in mm; and A, the area of faintest stellar images in arcmin^2. The radial range of each bin is given in arcmin; f_c is the number of stars per arcmin^2 after background subtraction but before correction for crowding. Where crowding corrections are necessary, they are calculated as in King *et al.* 1968 and are given in parentheses. These numbers are the logarithms of multiplicative factors and should be added directly to the uncorrected entries in the table. For example, for Plate ATT− of NGC 1818, the first entry is 1.63, the crowding correction is 0.06, and the corrected value of log f_c is 1.69. The values of f_b are background densities (numbers of stars per arcmin^2), and the values of log f_0 are the relative shifts required to align the profiles from the individual plates. The symbols correspond to those plotted in the lower panels (*b*) of Figs. 1–10. All logarithms are to base 10.

REFERENCES

Avni, Y. 1976, *Ap. J.*, **210**, 642.
Becker, S. A., and Iben, I. 1979, *Ap. J.*, **232**, 831.
Bernard, A., and Bigay, J. H. 1974, *Astr. Ap.*, **33**, 123.
Blitz, L., and Glassgold, A. E. 1982, *Ap. J.*, **252**, 481.
Bok, B. J., and Bok, P. F. 1960, *M.N.R.A.S.*, **121**, 531.
———. 1962, *M.N.R.A.S.*, **124**, 435.
Brunish, W., 1981, Ph.D. thesis, University of Illinois.
Carignan, C., and Freeman, K. C. 1985, *Ap. J.*, **294**, 494.
Chiosi, C. 1986, private communication.
Chiosi, C., Bertelli, B., and Bressan, A. 1986, *Mem. Soc. Astr. Italiana*, **57**, 507.
Chiosi, C., and Pigatto, L. 1986, *Ap. J.*, **308**, 1.
Chun, M. S. 1978, *A.J.*, **83**, 1062.
Cohen, J. G. 1982, *Ap. J.*, **258**, 143.
Cohen, R., Montani, J., and Rubio, M. 1984, in *IAU Symposium 108, Structure and Evolution of the Magellanic Clouds*, ed. S. van den Bergh and K. de Boer (Dordrecht: Reidel), p. 401.
Conti, P. S., Garmany, C. D., and Massey, P. 1986, *A.J.*, **92**, 48.
DaCosta, G. S. 1982, *A.J.*, **87**, 990.
de Vaucouleurs, G. 1960, *Ap. J.*, **131**, 574.
Eggen, O. J. 1965, in *Stars and Stellar Systems*, Vol. **5**, *Galactic Structure*, ed. A. Blaauw and M. Schmidt (Chicago: University of Chicago Press), p. 111.
———. 1984, *A.J.*, **89**, 1350.
Elmegreen, B. G. 1983, *M.N.R.A.S.*, **203**, 1011.
Elson, R. A. W., and Fall, S. M. 1985*a*, *Ap. J.*, **299**, 211.
———. 1985*b*, *Pub. A.S.P.*, **97**, 692.
Elson, R. A. W., and Freeman, K. C. 1985, *Ap. J.*, **288**, 521.
Elson, R. A. W., Hut, P., and Inagaki, S. 1987, *Ann. Rev. Astr. Ap.*, in press.
Feast, M. W. 1964, *M.N.R.A.S.*, **127**, 195.
Feitzinger, J. V. 1979, in *Photometry, Kinematics and Dynamics of Galaxies*, ed. D. S. Evans (Austin: University of Texas Press), p. 435.
Freeman, K. C. 1970, *Ap. J.*, **160**, 811.
———. 1974, in *ESO/SRC/CERN Conf. on Research Programmes for the New Large Telescopes*, ed. A. Reiz, p. 177.
———. 1977, in *The Evolution of Galaxies and Stellar Populations*, ed. B. M. Tinsley and R. B. Larson (New Haven: Yale University Observatory), p. 133.
Freeman, K. C., Illingworth, G. D., and Oemler, A. 1983, *Ap. J.*, **272**, 488.
Frenk, C. S., and Fall, S. M. 1982, *M.N.R.A.S.*, **199**, 565.
Gordon, K. C., and Kron, G. E. 1983, *Pub. A.S.P.*, **95**, 461.
Graham, J. A. 1982, *Pub. A.S.P.*, **94**, 244.
Hanes, D. A., and Brodie, J. P. 1985, *M.N.R.A.S.*, **214**, 491.
Heckman, T. M. 1974, *A.J.*, **79**, 1040.
Henon, M. 1973, in *Dynamical Structure and Evolution of Stellar Systems*, ed. L. Martinet and M. Mayor (Geneva: Geneva Observatory), p. 183.
Herbst, W., and Miller, D. P. 1982, *A.J.*, **87**, 1478.
Hodge, P. W. 1983, *Ap. J.*, **264**, 470.
Iben, I. 1965, *Ap. J.*, **142**, 1447.
———. 1966*a*, *Ap. J.*, **143**, 483.
———. 1966*b*, *Ap. J.*, **143**, 505.
———. 1966*c*, *Ap. J.*, **143**, 516.
———. 1967, *Ap. J.*, **147**, 624.
Iben, I., and Renzini, A. 1983, *Ann. Rev. Astr. Ap.*, **21**, 271.
Illingworth, G. 1976, *Ap. J.*, **204**, 73.
Illingworth, G., and Illingworth, W. 1976, *Ap. J. Suppl.*, **30**, 227.
Inagaki, S., and Saslaw, W. C. 1985, *Ap. J.*, **292**, 339.
Jones, B. F. 1970, *A.J.*, **75**, 563.
Jones, B. F. 1971, *A.J.*, **76**, 470.
Keenan, D. W. 1981*a*, *Astr. Ap.*, **95**, 334.
———. 1981*b*, *Astr. Ap.*, **95**, 340.
Kerr, F. J., and de Vaucouleurs, G. 1955, *Australian J. Phys.*, **8**, 508.
King, I. 1962, *A.J.*, **67**, 471.
———. 1966, *A.J.*, **71**, 64.
King, I., Hedemann, E., Hodge, S. M., and White, R. E. 1968, *A.J.*, **73**, 456.
Lada, C. J., Margulis, M., and Dearborn, D. 1984, *Ap. J.*, **285**, 141.
Mathieu, R. D. 1983, *Ap. J.* (*Letters*), **267**, L97.
———. 1984, *Ap. J.*, **284**, 643.
———. 1985, in *IAU Symposium 113, Dynamics of Star Clusters*, ed. J. Goodman and P. Hut (Dordrecht: Reidel), p. 427.
McClure, R. D., *et al.* 1986, *Ap. J.* (*Letters*), **307**, L49.
McGee, R. X., and Milton, J. A. 1966, *Australian J. Phys.*, **19**, 343.
McGlynn, T. A. 1984, *Ap. J.*, **281**, 13.
Mengel, J. G., Sweigart, A. V., Demarque, P., and Gross, P. G. 1979, *Ap. J. Suppl.*, **40**, 733.
Nelson, M., and Hodge, P. 1983, *Pub. A.S.P.*, **95**, 5.
Pels, G., Oort, J. H., and Pels-Kluyver, H. A. 1975, *Astr. Ap.*, **43**, 423.
Persson, S. E., Aaronson, M., Cohen, J. G., Frogel, J. A., and Matthews, K. 1983, *Ap. J.*, **266**, 105.
Renzini, A., and Buzzoni, A. 1986, in *The Spectral Evolution of Galaxies*, ed. C. Chiosi and A. Renzini (Dordrecht: Reidel), p. 195.
Rholfs, K., Kreitschmann, J., and Feitzinger, J. V. 1984, in *IAU Symposium 108, Structure and Evolution of the Magellanic Clouds*, ed. S. van den Bergh and K. de Boer (Dordrecht: Reidel), p. 395.
Robertson, J. W. 1974*a*, *Astr. Ap. Suppl.*, **15**, 261.
———. 1974*b*, *Ap. J.*, **191**, 67.
Scalo, J. M. 1986, *Fund. Cosmic Phys.*, **11**, 1.
Schlesinger, B. M. 1969, *Ap. J.*, **157**, 533.
Schommer, R. A., Olszewski, E. S., and Aaronson, M. 1984, *Ap. J.* (*Letters*), **285**, L53.
Searle, L. 1984, in *IAU Symposium 108, Structure and Evolution of the Magellanic Clouds*, ed. S. van den Bergh and K. de Boer (Dordrecht: Reidel), p. 13.
Searle, L., Sargent, W. L. W., and Bagnuolo, W. G. 1973, *Ap. J.*, **179**, 427.
Seitzer, P. 1983, Ph.D. thesis, University of Virginia.
———. 1985, in *IAU Symposium 113, Dynamics of Star Clusters*, ed. J. Goodman and P. Hut (Dordrecht: Reidel), p. 343.
Shapiro, S. L., and Lightman, A. P. 1976, *Nature*, **262**, 743.
Spitzer, L., and Hart, M. H. 1971, *Ap. J.*, **166**, 483.
Spitzer, L., and Shapiro, S. L. 1972, *Ap. J.*, **173**, 529.
Stahler, S. W. 1985, *Ap. J.*, **293**, 207.
Stothers, R. L. 1963, *Ap. J.*, **138**, 1074.
———. 1972, *Ap. J.*, **175**, 431.
Toomre, A. 1963, *Ap. J.*, **138**, 385.
van Albada, T. S. 1982, *M.N.R.A.S.*, **201**, 939.
van den Bergh, S. 1981, *Astr. Ap. Suppl.*, **46**, 79.
van den Bergh, S., and Hagen, G. L. 1968, *A.J.*, **73**, 569.
van Leeuwen, F. 1980, in *IAU Symposium 85, Star Clusters*, ed. J. E. Hesser (Dordrecht: Reidel), p. 157.
Webbink, R. F. 1985, in *IAU Symposium 113, Dynamics of Star Clusters*, ed. J. Goodman and P. Hut (Dordrecht: Reidel), p. 541.
Woolley, R. 1965, in *Stars and Stellar Systems*, Vol. **5**, *Galactic Structure*, ed. A. Blaauw and M. Schmidt (Chicago: University of Chicago Press), p. 85.
Yamanaka, J. 1986, private communication.

REBECCA A. W. ELSON: Institute for Advanced Study, Princeton, NJ 08540

S. MICHAEL FALL: Space Telescope Science Institute, 3700 San Martin Drive, Baltimore, MD 21218

KENNETH C. FREEMAN: Mount Stromlo and Siding Spring Observatory, Private Bag, Woden P.O., A.C.T. 2606, Australia